RESEARCH CENTER

AMERICAN OPTICAL COMPANY

Southbridge, Massachusetts

ESR AND OPTICAL ABSORPTION STUDIES OF TRANSITION METAL IONS AND COLOR CENTERS IN GLASS

SEMI ANNUAL TECHNICAL REPORT
NUMBER ONE

1 October 66 - 31 March 67

ARPA Order No. 306
Contract No. N00014-67-C-0186

Prepared by

Research Division
American Optical Company
Southbridge, Massachusetts

Project Manager - Dr. Elias Snitzer
Project Scientist - Robert J. Landry
Project Scientist - Joseph T. Fournier

This research is part of Project DEFENDER under the joint sponsorship of the Advanced Research Projects Agency, Department of Defense and the Office of Naval Research.

ABSTRACT

The theory of zero field ESR measurements of an S = 3/2 system is considered, including spectrometer considerations. A brief discussion of an experimental problem associated with temperature dependent ESR intensity measurements of broad powder spectra is included along with a proposed solution. The optical absorption and ESR spectra of Mo^{5+} and Cu^{2+} in glass, in the concentration range 0.1-16.0 wt. % MoO_3 and CuO, respectively, were investigated. In both cases, the ESR spectra are found to be concentration dependent. For isolated Cu^{2+}, the axial spin Hamiltonian parameters obtained are: $g_{\parallel} = 2.335 \pm 0.002$, $g_{\perp} = 2.050 \pm 0.001$, $A_{\parallel} = 155 \pm 1 \times 10^{-4}\,cm^{-1}$, and $A_{\perp} = 22.7 \pm 0.1 \times 10^{-4}\,cm^{-1}$. ESR and optical absorption spectra of Mo^{3+} in a phosphate glass are shown. The value of the crystal field splitting parameter Δ is 22,000 cm^{-1}, about 52% greater than the value of 14,500 cm^{-1} for isoelectronic Cr^{3+} in the same base glass.[1] The spin resonance spectra of Cr^{3+} and Mo^{3+} are compared, from which it is concluded that they are similarly accommodated in the glass. Their local environments appear to be identical. A technique is described which allows for a precise determination of the activation spectrum for production of permanent color center defects by ultraviolet light. The activation spectrum for induced permanent color center defects in a laser base glass is presented. The spectrum has a peak at 214 nm and has a full width at half maximum of 13.0 nm. An upper bound of 240 nm for the activation spectrum for short lived laser Q-switching color center defects is demonstrated.

Preliminary results of a theoretical investigation of the electronic structure of color center defects associated with network-forming tetrahedra are reported. A silicon-oxygen tetrahedron with a single non-bridging oxygen is chosen as the initial subject for study. The molecular structure of the tetrahedron is described in the valence bond picture, and a formal discussion of valence bond theory is presented. The role of π bonding in the tetrahedron is considered. It is shown that localized π hybrids can be constructed from Si 3d and 4f atomic orbitals, and the details of a group theoretical procedure for determining these hybrids are presented. Finally, some computational aspects of the problem are discussed.

CONTENTS

FIGURE ILLUSTRATIONS PAGE

1. INTRODUCTION

Fundamental studies of transition metal ions and color center defects in glass are of importance because their presence can seriously affect the optical properties of laser glass. Further, the nature of these centers in glass for the most part is not well understood.

The work performed to date on this contract can be classified into studies of transition metal ions in glass, experimental studies of color center defects in glass, and theoretical investigations of color center defects in glass.

The program of transition metal ions in glass includes a continuation of a study of Cr^{3+} which had been initiated prior to this study, and studies of other transition metal ions in glass. Previous investigations of Cr^{3+} have allowed for an estimate of the zero field splitting parameter $|2D|$.[1] In this work, attempts will be made to obtain a direct measurement of the distribution function in the zero field splitting. To date, the theory of such measurements for an $S = 3/2$ system has been considered, and spectrometers have been designed. The equipment has been purchased and is in the process of being assembled.

The existence of exchange coupled Cr^{3+} ion pairs in a phosphate glass was also demonstrated in the earlier study.[1] In this work, attempts to measure the magnitude of the isotropic exchange coupling constant $|J|$ have been initiated. The two studies above are described in Sections 2.1 and 2.2, respectively.

Investigations of other transition metal ions in glass are concerned with studies of Mo^{5+}, Mo^{3+}, and Cu^{2+}. A description of this part of the program is contained in Section 2.3

Experimental color center defect studies in glass includes investigations of both permanent and relatively short lived color centers, and are described in Section 3.

Finally, description of a theoretical investigation of the electronic structure of color center defects associated with network-forming tetrahedra is contained in Section 4.

2. TRANSITION METAL IONS IN GLASS

2.1 ZERO FIELD SPLITTING OF ISOLATED Cr^{3+} IONS IN GLASS

The optical absorption and electron spin resonance (ESR) spectra of isolated Cr^{3+} ions in an aluminum-zinc-phosphate glass can be adequately accounted for if the Cr^{3+} ions are taken to reside in a crystal field potential of cubic symmetry with a small amount of axial and orthorhombic distortion.[1] Since the ground state term for Cr^{3+} in octahedral cubic symmetry is the orbital singlet $^4\Gamma_2$, the ESR spectrum can be described by the spin Hamiltonian for axial symmetry,

$$H_s = DS^2_Z + g_e \beta \vec{H}_{DC} \cdot \vec{S} + g_e \beta \vec{H}_{RF} \vec{S}, \qquad (1)$$

where D is the axial crystal field parameter, g_e is the free electron g-value, β is the Bohr magneton, H_{DC} is the DC magnetic field intensity, H_{RF} is the microwave RF magnetic field intensity, and S is the electronic spin angular momentum operator. The second and third terms in eq. (1) are first order terms and are time independent and time dependent respectively. The action of DS^2_z on the $^4\Gamma_2$ level is to split the four fold spin degenerate level into two Kramers doublets characterized by $M_s = \pm 3/2$ and $M_s = \pm 1/2$ and separated in energy by $|2D|$, commonly referred to as the zero field splitting. In a phosphate glass $|2D|$ has been estimated to be in the range 0.3 to 1.0 cm^{-1}.[1] The transitions of interest in zero field splitting measurements are those between the doublets. Attention will therefore be restricted only to these transitions in the following analysis. In eq. (1),

$$\vec{H}\cdot\vec{S} = H_X S_X + H_Y S_Y + H_Z S_Z$$

can be written as

$$\vec{H}\cdot\vec{S} = 1/2(H_- S_+ + H_+ S_-) + H_Z S_Z,$$

where the raising and lowering operators are defined by the relationship $O_\pm = O_X \pm iO_Y$. H_s then takes the form,

$$H_s = DS^2_Z + 1/2\, g_e\beta\, (H_{DC-} S_+ + H_{DC+} S_-) + H_{DCZ} S_Z$$

$$(H_{RF-} S_+ + H_{RF+} S_-) + H_{RFZ} S_Z. \qquad (2)$$

From the terms involving H_{DC} in the above equation, it can be seen that for arbitrary orientation of the DC magnetic field

with respect to the crystalline field Z axis shown in Fig. 1, the $M_s = \pm 1/2$ levels become intermixed, whereas the $M_s = \pm 3/2$ levels do not become intermixed. This is so since the raising and lowering operators S_+ and S_- can connect the matrix elements of $M_s = \pm 1/2$ but cannot connect the matrix elements of $M_s = \pm 3/2$. The first four terms in eq. (2) give rise to the energy level scheme shown in Fig. 2. It should be noted that the energy scheme for $-H_{DC}$ (H_{DC} in the opposite sense to $+H_{DC}$) is the mirror image of $+H_{DC}$ with the labeling of the levels within the doublets interchanged.

In eq. (2), the operator $H_{RF}\, S_Z$ cannot connect states which differ by $\Delta M_s = \pm 1$ and so cannot give rise to transitions between the doublets. Since this term need not be considered, it will be dropped. H_{RF-} and H_{RF+} are the proper rotating and counter rotating components of circular polarization, respectively. For the transitons of interest, either one of these components can be chosen since they both give rise to the same physical situation as will be shown below. For convenience and illustration, the proper component will be chosen. When specialized to this case, the spin Hamiltonian becomes,

$$H_s = DS^2_Z + \frac{1}{2} g_e \beta (H_{DC+} S_- + H_{DC-} S_+) + \frac{1}{2} g_e \beta H_{DCZ} S_Z + \frac{1}{2} g_e \beta H_{RF-} S_+ . \qquad (3)$$

The transition probability for transitions between the two doublets is proportional to the square of the matrix element of the last term in eq. (3),

$$|\langle f|S_+|i\rangle|^2 \text{ where } \quad i = \pm 1/2, \quad f = \pm 3/2 .$$

It is obvious that the matrix elements connecting $f = -3/2$ to $i = \pm 1/2$ are zero. Hence, transition from ϕ_1 and ϕ_2 to ϕ_3 are disallowed, and only two transitions from ϕ_1 and ϕ_2 to ϕ_4 are allowed as shown in Fig. 2. A typical plot of the transition frequency for the two resulting transitions as a function of H_{DC} would appear as shown in Fig. 3.[2] From Fig. 3, it can be seen that the two transitions cross in zero field. Further, if magnetic field modulation is employed while the microwave frequency is swept through the crossover point in the zero field, the familiar first derivative of the paramagnetic absorption will be obtained.

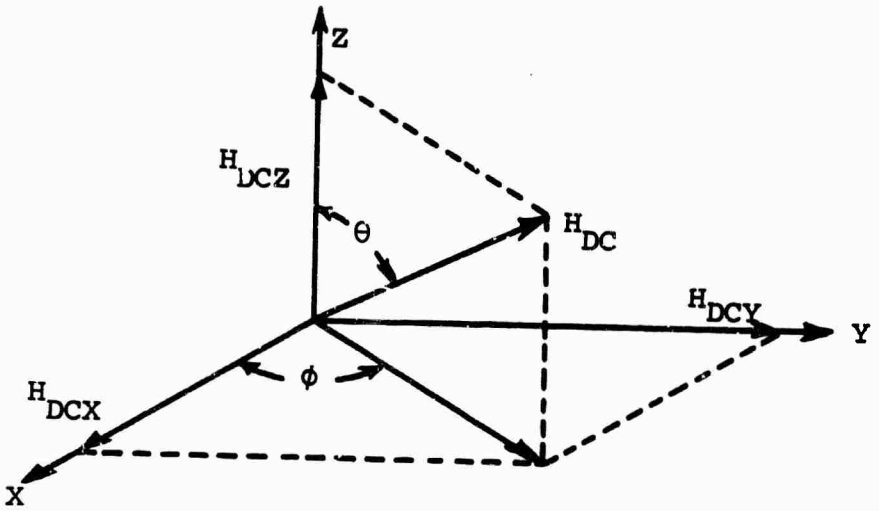

Fig. 1. Orientation of DC magnetic field with respect to crystalline symmetry axes.

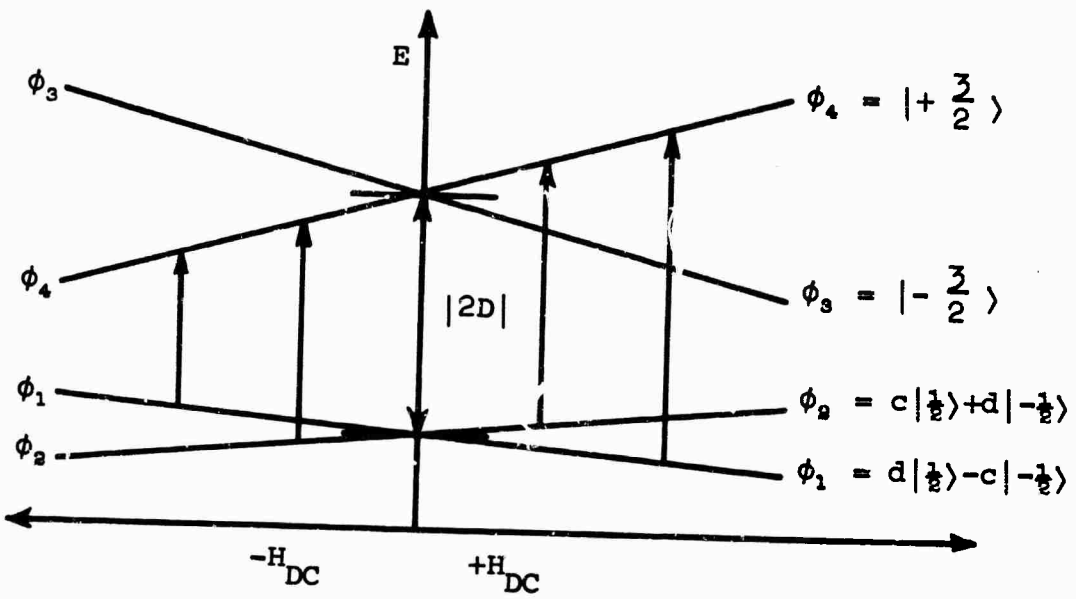

Fig. 2. Energy level scheme for an S = 3/2 system with zero field splitting |2D| for arbitrary orientation of DC magnetic field.

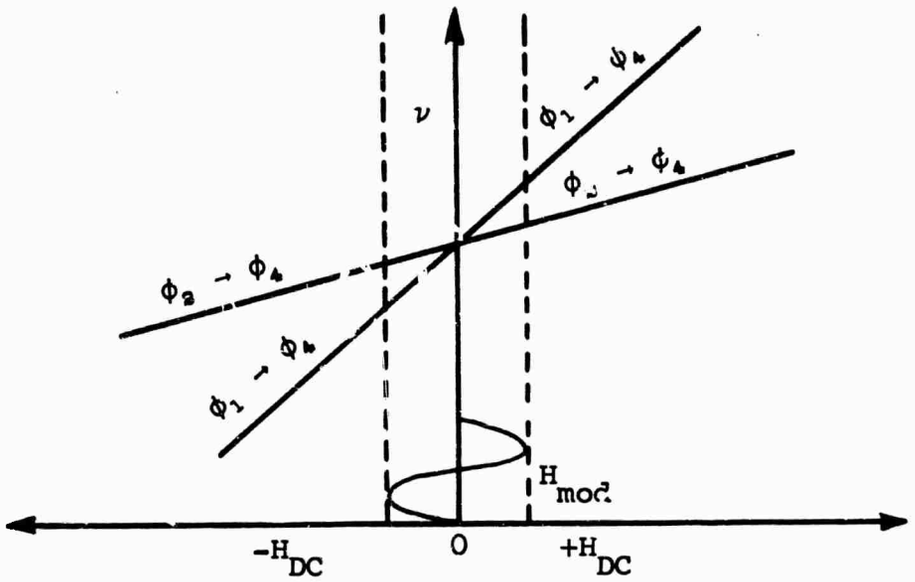

Fig. 3. Characteristic plot of the transition frequency ν vs. H_{DC} for transitions $\phi_1 \rightarrow \phi_4$ and $\phi_2 \rightarrow \phi_4$.

If the counter rotating component of microwave magnetic field had been chosen, transition probability would have been proportional to the square of the matrix element of S_- instead of S_+, resulting in transitions only from ϕ_1 and ϕ_2 to ϕ_3. Thus, the mirror image about $H_{DC} = 0$ would be obtained for the plot of transition frequency vs. H_{DC} in Fig. 3.

Since magnetic field modulation can be meaningfully used and since the sensitivity of a spectrometer is greatly increased by the use of phase sensitive detection, a straight-through zero field splitting ESR spectrometer utilizing 10 kc magnetic field modulation was designed, the block diagram of which is shown in Fig. 4. The salient features of this spectrometer include a frequency stabilized backward wave oscillator (B.W.O.) which covers the frequency range 18-26 kMc/sec, a direct reading rotating vane variable attenuator, a direct reading transmission cavity, a sample absorption cell, a 10 kc/sec oscillator, and a low noise high gain 10 kc/sec amplifier phase sensitive detector. The B.W.O. power supply and A.F.C. units were purchased from Micro-Now Corporation in Chicago, and are designed so that three plug-in type B.W.O. units covering the frequency range 12-40 kMc/sec can be easily interchanged.

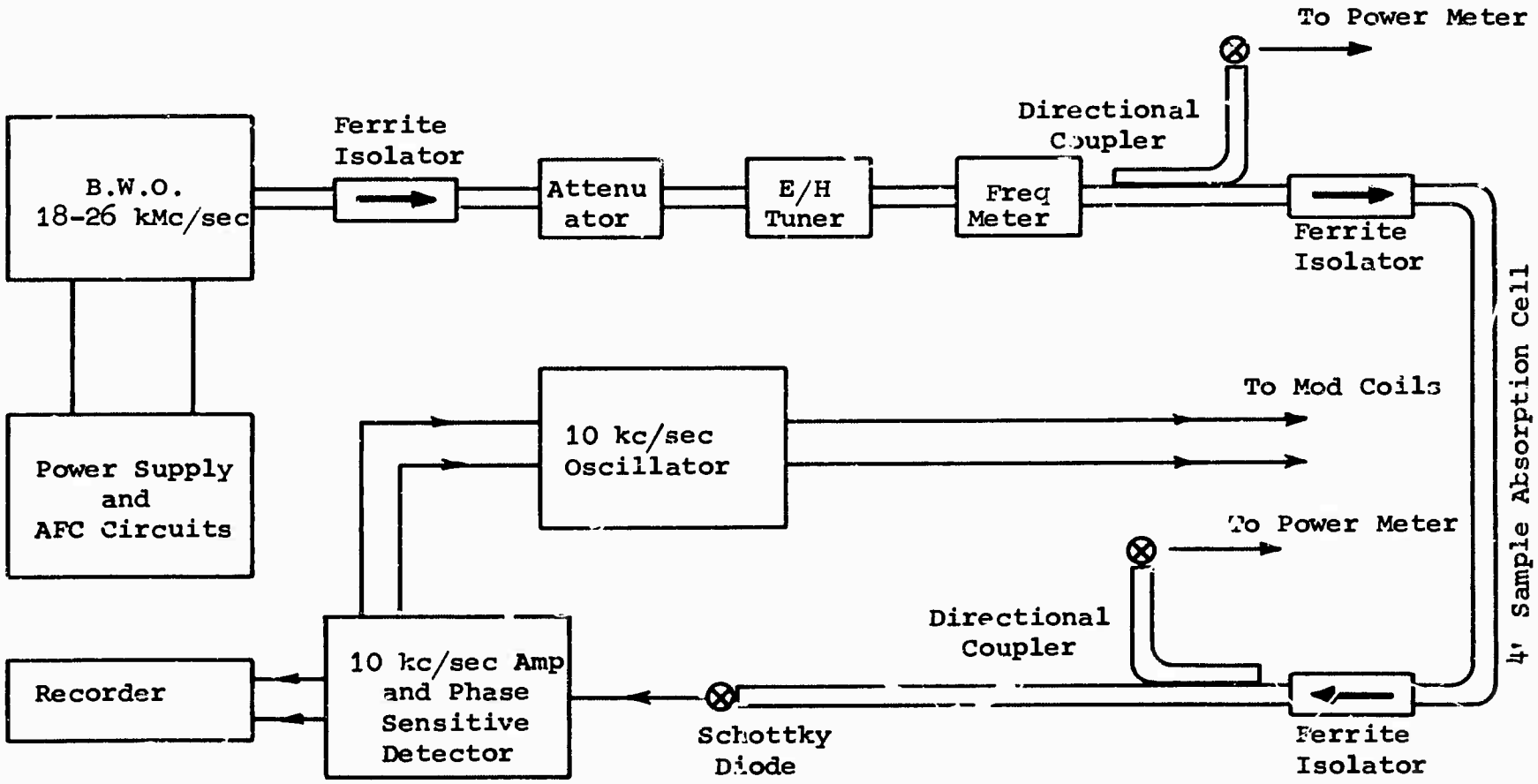

Fig. 4. Block diagram of zero field splitting ESR spectrometer.

Further, the above spectrometer can be easily converted to a more sensitive bridge type spectrometer with the addition of two hybrid tees and two matched absorption cells.

2.2 EXCHANGE COUPLED Cr^{3+} PAIRS IN GLASS

As the concentration of chromium in the aluminum-zinc-phosphate glass is increased, the Cr^{3+} ions form exchange coupled pairs.[1] The temperature dependence of the intensity of the ESR spectrum, relative to a spin 1/2 system is given by

$$I(T) \propto \frac{2e^{-J/kT} + 4e^{-3J/kT} + 6e^{-6J/kT}}{1 + 3e^{-J/kT} + 5e^{-3J/kT} + 7e^{-6J/kT}} \qquad (4)$$

where J is the isotropic exchange coupling constant. Thus, from a study of the temperature dependence of the ESR intensity, it may be possible to determine the magnitude of J. Since 100 cps magnetic field modulation is employed, the first derivative of the ESR spectrum is obtained. Further, since the intensity is proportional to the area under the absorption curve, a tedious and cumbersome double numerical integration must be carried out. Because the ESR spectrum of the paired ions is very broad (over 300 gauss at 9.49k Mc/sec), small errors introduced in the first derivative curve due to baseline drift become greatly magnified when carried through the double integration procedure. Experimentally, it was found that it is extremely difficult and very time consuming to obtain a spectrum which did not contain an intolerable amount of error. The error introduced by baseline drift is caused by a $\vec{J}x\vec{B}$ interaction of eddy currents in the brass cavity walls due to 100 cps magnetic field modulation with the slowly varying DC magnetic field. This baseline drift can be minimized by rotation of the DC electromagnet with respect to the brass cavity walls. The adjustment required is a fine one and is almost impossible to accomplish on the broad first derivative curve Therefore, an integrating circuit has been designed which will allow for a direct recording of the absorption. Recording and adjustments can then be made until the baseline drift has been completely eliminated from the absorption curve.

Experiments will be continued as soon as all electronic components have been received.

2.3 ESR AND OPTICAL ABSORPTION STUDIES OF Mo^{5+}, Mo^{3+}, AND Cu^{2+} IN GLASS

2.3.1 EXPERIMENTAL METHODS

The optical absorption spectra were measured on a Cary Model 14 recording spectrophotometer. Glass samples in the form

of polished flats 10 mm by 20 mm with thicknesses from 0.1 to 4.0 mm were investigated at room temperature in the wavelength range 300 to 1500 nm. ESR measurements at 9.49 kMc/sec were performed on a superheterodyne spectrometer utilizing a rectangular cavity operating in the TE_{102} mode with 100 cps magnetic field modulation. The ESR samples were flats of 0.1 mm thickness and were placed in the region of maximum microwave magnetic field.

2.3.2 Mo^{5+}

The nature of the local environment of molybdenum in glass is of considerable interest since it is isoelectroric with chromium. A series of aluminum-zinc-phosphate glasses containing MoO_3 in the concentration range (0.1 - 16.0 wt. %) were fabricated. Attempts to increase the MoO_3 concentration beyond 16.0 wt. % resulted in devitrification. The glasses have base composition of approximately 90 wt. % $Al(PO_3)_3$, 10 wt.% ZnO, and 2 wt.% Sb_2O_3. The antimony was added to the glass melt in order to make the melting conditions more reducing for molybdenum. Both the ZnO and MoO_3 starting materials were of reagent grade. The $Al(PO_3)_3$ was of lesser quality. However, optical and ESR spectra of a glass sample with no molybdenum content show no absorptions in the regions of interest.

The ESR spectra of the above glasses show only the presence of Mo^{5+}, and is similar in character to the ESR spectrum of its isoelectronic Cr^{5+} counterpart in the glassy state.[3,4] The optical transmission spectrum of a blue glass sample doped with 0.5 wt. % MoO_3 is shown in Fig. 5. There are some very small changes in the optical spectrum in the region of 300 nm as the concentration of MoO_3 is increased. Since Mo^{5+} and Mo^{6+} both have absorptions in the charge transfer band, the small changes observed in the optical spectra might possibly be accounted for by a change in the ratio of Mo^{5+} to Mo^{6+}. Further investigations of the changes in the optical spectra as a function of increasing concentration should be undertaken in order to clarify this point. However, this point need not present any difficulty in the interpretation of the ESR spectra since only Mo^{5+} is paramagnetic with $S = 1/2$.

The ESR spectra of glass samples doped with 0.1%, 1.0%, 4.0% and 16.0%, all in wt. % MoO_3 are shown in Fig. 6. As can be seen from Fig. 6, there is a definite concentration dependence; the lowest concentration spectrum presumably arising mostly from isolated ions, and the highest concentration spectrum presumably arising mostly from interacting pairs of Mo^{5+} ions. The spectrum of samples with intermediate concentrations appear to consist of

a superposition of lines from both isolated and interacting pair systems.

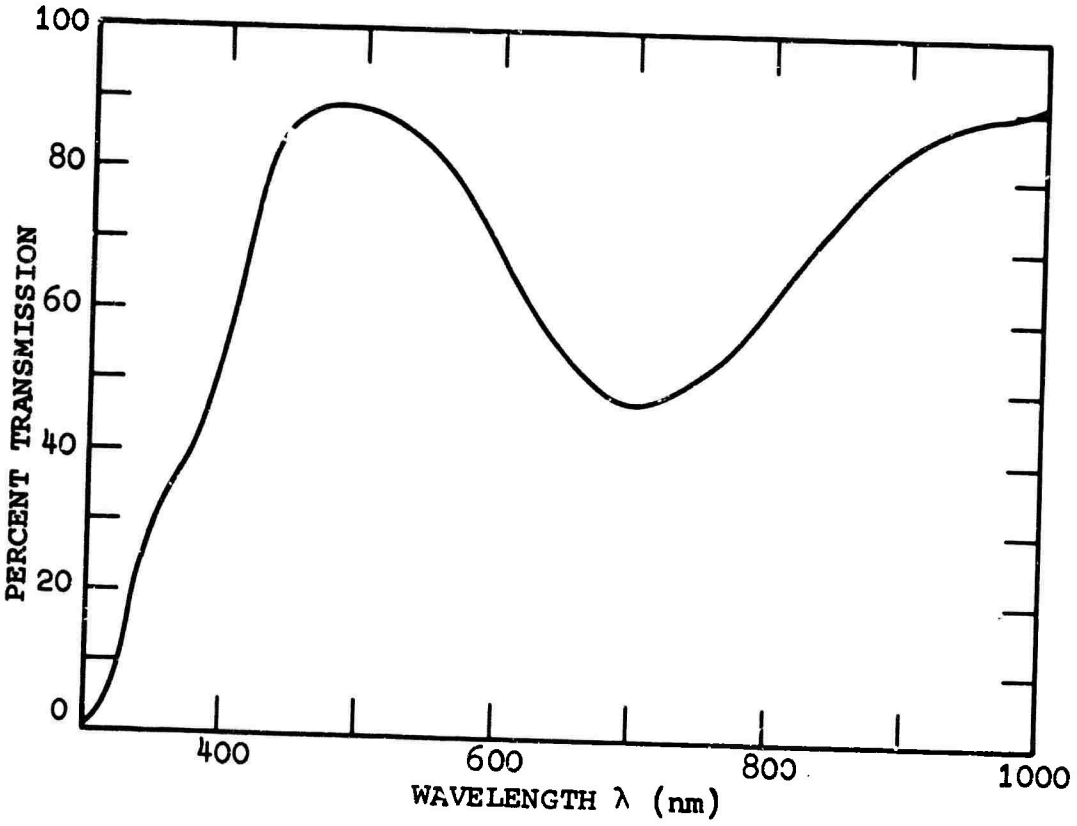

Fig. 5. Optical transmission spectrum of a 1 mm thick aluminum-zinc-phosphate glass doped with 0.5 wt. % MoO_3 showing the absorption due to Mo^{5+}.

Both nuclear isotopes, ^{95}Mo and ^{97}Mo have nuclear spin 5/2, magnetic moments -0.9290 and -0.9485 nuclear magnetons, and are 15.7 and 9.45 percent naturally abundant, respectively.[6] Since their nuclear magnetic moments are approximately the same, it is impossible in the powder spectrum to separate the hyperfine structure resulting from each. For analysis of the powder spectrum, 25% of the molybdenum ions can thus be considered to have nuclear spin 5/2. The resulting ESR spectrum of this system in a cubic field would consist of six equally spaced isotropic hyperfine lines centered about a larger isotropic line which arises from the isotopes which have zero nuclear spin. Further, the hyperfine lines should have approximately the same intensity and should be three times smaller in intensity than the main central line. The ESR spectrum of the sample shown in Fig. 6a shows only a partially

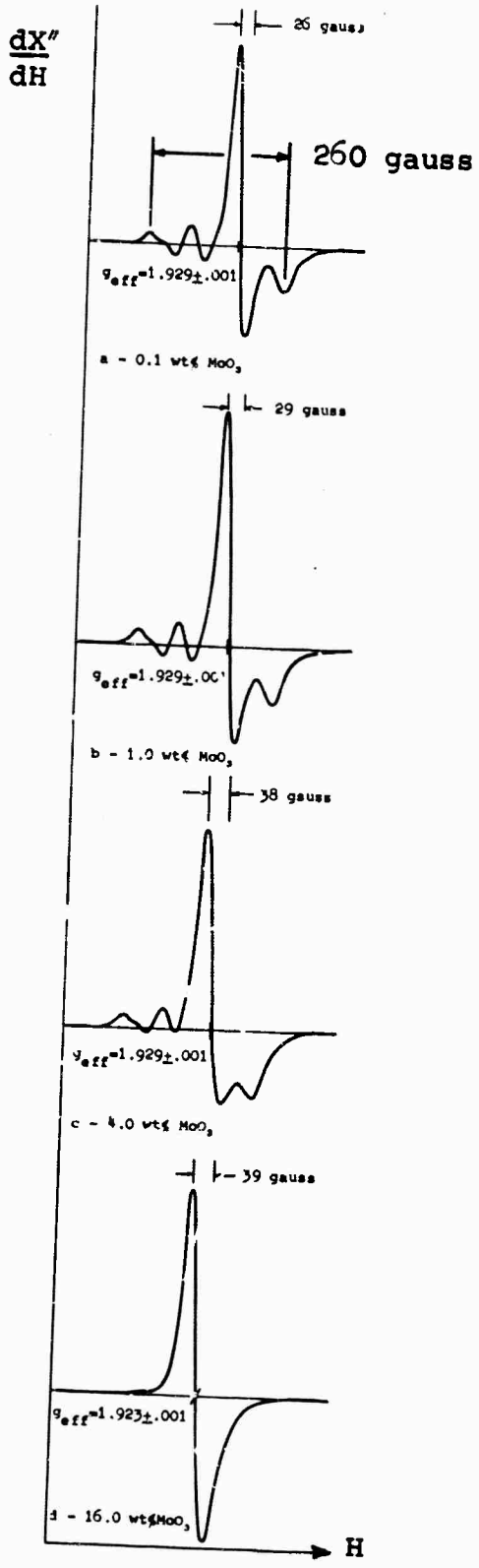

Fig. 6. Concentration dependence of 9.49 kMc/sec ESR spectra of Mo^{6+} in a phosphate glass doped with: a, 0.1 wt. %; b, 1.0 wt. %; c, 4.0 wt. %; and d, 16.0 wt. % MoO_3 at 77°K.

resolved hyperfine structure and further indicates an expected g value anisotropy. The spectrum of Mo^{5+} in this glass appears to be somewhat similar to its spectrum in other materials.[4,6] Plans for the future include obtaining the ESR spectrum of the sample which contains 0.1 wt. % MoO_3 at 24 kMc/sec. Since the spectrum at 24 kMc/sec may be much better resolved, it may be more meaningfully analyzed. For this reason no attempt has been made to analyze the spectrum at 9.49 kMc/sec.

As can be seen from Fig. 6 (b-d), the systems of lines which arise from isolated Mo^{5+} ions and interacting pairs both occur in the same region of magnetic field at 9.49 kMc/sec. Further, since only 25% of the Mo^{5+} ions have nuclear spins, the resulting powder spectrum consists of the superpostion of resonances from five non-identical systems. Because of these complications, interpretation of the changes in the ESR spectra is difficult. The changes in the spectrum could be due to dipolar broadening, exchange interactions, or some combination of these.

Dipolar broadening can occur when the paramagnetic ions get close enough together such that the effective magnetic fields seen by the ions is the sum of the external magnetic field and the magnetic fields produced by the nearby paramagnetic dipole neighbors. The individual ions then see different effective magnetic fields which results in a broadening of the ESR line. Dipolar broadening can also occur when nearby ions precess with the same Larmor frequency. An interaction occurs which causes their spin orientation to change, thereby reducing the average lifetime of the ions in a given state. This manifests itself in a broadening of the ESR line. On the other hand, an exchange interaction between paramagnetic ions is electrostatic in nature and is connected with the overlap of orbital wave functions.

If the two basic systems consist of exchange coupled and isolated ions, it may be possible to separate the spectra arising from each by performing additional ESR experiments at 2.0 kMc/sec and at 24 kMc/sec. On the other hand, if the changes in the spectra arise from a dipolar broadening mechanism, it should not be possible to separate the spectra arising from the isolated and interacting pair systems by changing the size of the microwave photon. This is so because in the latter case all paramagnetic species still have effective spin of 1/2; whereas in the former case the exchange coupled pairs have effective spin of 1 and the isolated ions have effective spin of 1/2. Plans for the future include additional ESR experiments at 2.0 kMc/sec and 24 kMc/sec.

2.3.3 Mo^{3+}

In order to obtain Mo^{3+} in this base glass. the sample which contained 0.5 wt. % MoO_3 was remade under more strongly reducing conditions. A small amount of carbon was added to the melt which was maintained in a nitrogen atmosphere. The optical transmission spectrum of the resulting 1 mm thick amber colored glass is shown in Fig. 7. The characteristics of the optical absorption spectrum of Mo^{3+} in this glass are similar to those of Cr^{3+} in a similar base glass.[1] The peaks in Fig. 7 are labeled by excited terms of a d^3 system in a cubic crystal field. As for Cr^{3+}, if the lowest energy peak is attributed to the ${}^4\Gamma_2 \rightarrow {}^4\Gamma_5$ transition, then $\Delta \cong 22{,}000\ cm^{-1}$. The value of the parameter Δ for Mo^{3+} is therefore about 52% greater than the value of 14,500 cm^{-1} for Cr^{3+}.[1]

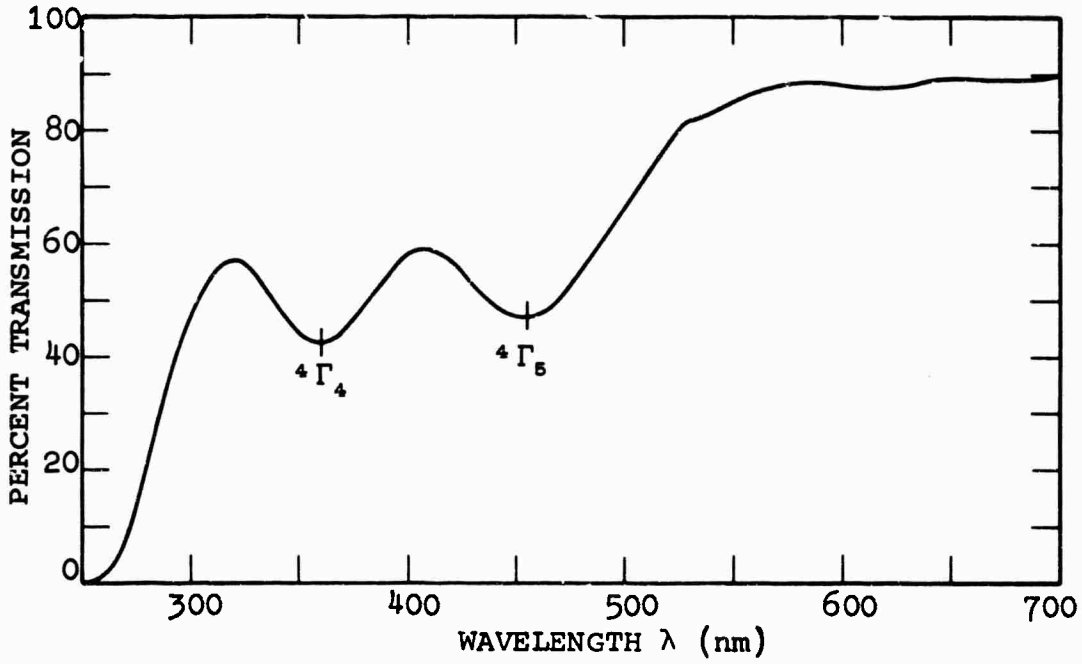

Fig. 7. Optical transmission spectrum of a 1 mm thick aluminum-zinc-phosphate glass doped with 0.5 wt. MoO_3 showing the absorption due to Mo^{3+}.

The ESR spectrum at 9.49 kMc/sec and at 77°K of the above sample is shown in Fig. 8b. The sharp line near $g_{eff} = 2$ is due to a small amount of Mo^{5+}. The presence of Mo^{5+} is just barely indicated in the transmission spectrum of Fig. 7. Since the line width of the ESR signal due to Mo^{3+} is about sixty times less than the line width of the ESR signal due to Mo^{3+}, the concentration of Mo^{5+} can only be a few percent of the total amount of

molybdenum in the glass. There may, however, be some additional molybdenum present in the non-paramagnetic $^{6+}$ valence state.

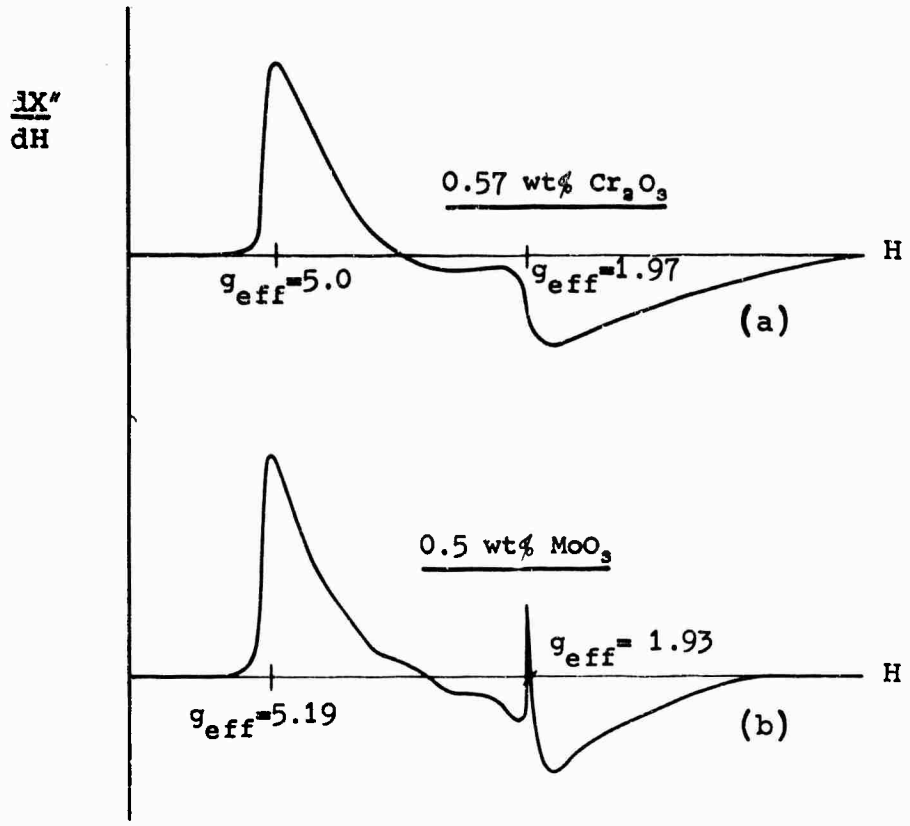

Fig. 8. ESR spectra of isoelectronic Mo^{3+} and Cr^{3+} at 9.49 kMc/sec and at 77°K in an aluminum-zinc-phosphate glass doped with: a, 0.57 wt. % Cr_2O_3 and b, 0.5 wt.% MoO_3. In both cases, the low field component of the ESR spectrum peaks near $g_{eff} = 5.0$. The small differences in shape may possibly be due to differences in unresolved hyperfine structure, small differences in concentration and small differences in their pairing characteristics.

For purposes of comparison, the ESR spectrum of a sample which contains 0.5 wt. % Cr_2O_3, all in the Cr^{3+} state, in a similar aluminum-zinc-phosphate glass is shown in Fig. 8a. The ESR spectra of both isolated Cr^{3+} and Mo^{3+} begin at about $g_{eff} = 5.9$, have a peak at about $g_{eff} = 5.0$, and in general appear to be quite similar. The nuclear isotope of chromium, ^{53}Cr is 9.55% naturally abundant, has nuclear spin I = 3/2, and a nuclear magnetic moment of -0.4735 nuclear magnetons.[5] The nuclear isotopes of molybdenum, ^{95}Mo and ^{97}Mo are 15.70% and 9.45% naturally abundant, have nuclear spin 5/2 and have nuclear magnetic moments of -0.9290 and -0.9485 nuclear magnetons, respectively.[5] Unresolved hyperfine structure gives rise to line broadening effects. Thus, the small differences observed in the ESR spectra of these ions may be partially due to

differences in unresolved hyperfine structure. Further, the ESR spectra of Cr^{3+} was found to be concentration dependent.[1] The concentration dependence of the ESR spectra of Mo^{3+} has not yet been investigated. Since the concentration of Mo^{3+} and Cr^{3+} in the spectra shown in Fig. 8 are different, the small changes may be partially due to concentration effects. Since the differences in the spectra are small and most likely caused by the effects cited above, and because of the nature of the analysis, the small differences can be ignored.[1] As for Cr^{3+}, analysis of the ESR and optical absorption spectra indicates zero field splittings in the range 0.3 through 1 cm^{-1}.[1]

From the similarities noted above it is also possible to conclude that the nature of the local environment of isolated Mo^{3+} and Cr^{3+} in the phosphate glass are quite similar if not identical. Since the ionic radii of Cr^{3+} and Mo^{3+} are 0.65Å and 0.68Å, respectively, the model proposed for the local environment of Cr^{3+} appears to apply equally well for Mo^{3+}.[1,7]

The valence states of molybdenum in glass are not easily controlled. Thus, a study program directed toward better understanding and greater control of its valence states in glass has been initiated. This study will involve fabrication and analysis of molybdenum in various types of base glass melted under various conditions. A controlled atmospheric furnace will be used in these studies. If and when control of the valence states of molybdenum has been achieved, an optical and ESR concentration dependent study of Mo^{3+} will be undertaken.

2.3.4 Cu^{2+}

A series of soda-lime-silicate glasses containing CuO in the concentration range (0.1 - 16.0 wt. %) were fabricated. Attempts to increase the CuO concentration beyond 16.0 wt. % resulted in devitrification. The glasses have base composition of approximately 68 wt. % $Si\,O_2$, 20 wt. % Na_2O and 12 wt. % CaO. The glasses were prepared in a globar furnace under oxidizing conditions. All starting materials were of reagent grade, and optical and ESR spectra of a glass sample with no copper content show no absorptions in the regions of interest. The optical transmission spectrum of a 1 mm thick blue colored glass sample doped with 0.5 wt. % CuO is shown in Fig. 9. As the concentration of CuO is increased, small changes occur in the transmission spectrum in the region of 300 nm. Since both Cu^{+} (d^{10}) and Cu^{2+} (d^{9}) have absorptions in the change transfer bands, the changes observed may possibly be accounted for by a change in the ratio of the concentration of Cu^{2+} to Cu^{+}. It should be pointed out

that the presence of both these valence states presents no difficulty in the interpretation of the ESR spectra since Cu^{+} is not paramagnetic. Further investigation of the changes in the optical spectra should be undertaken in order to clarify this point.

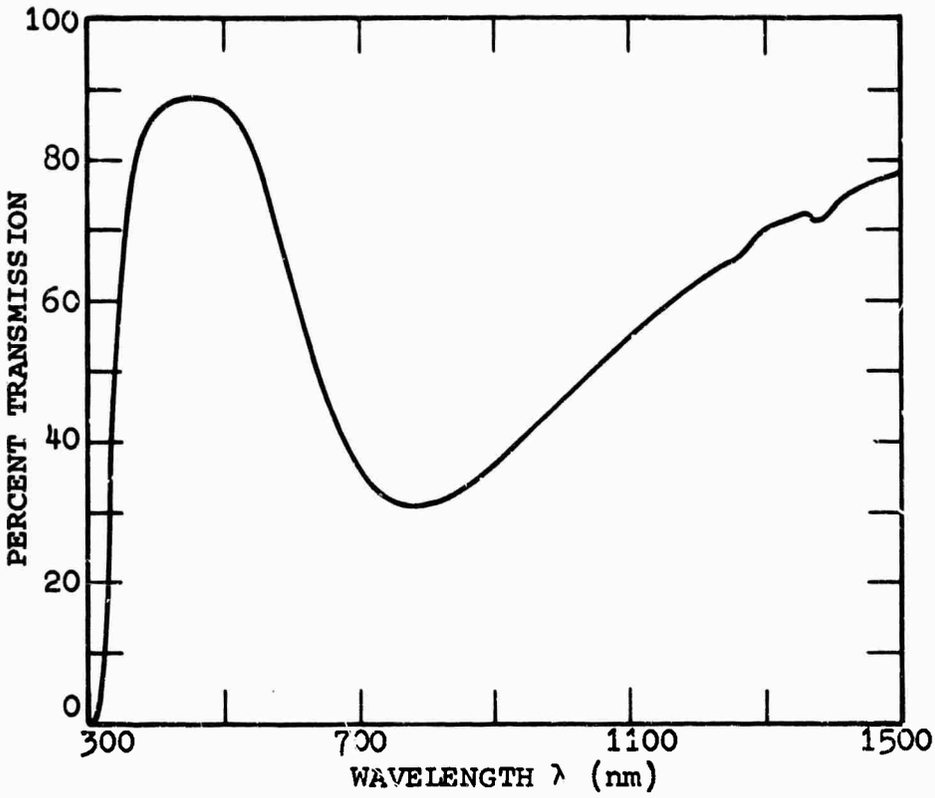

Fig. 9. Optical transmission spectrum of a 1 mm thick soda-lime-silicate glass doped with 0.5 wt. % Cu O showing the absorption due to Cu^{2+}.

The concentration dependence of the ESR spectra of the Cu^{2+} ($S = 1/2$; $I = 3/2$) doped samples is shown in Fig. 10. As can be seen from Fig. 10, there is a definite concentration dependence, the lowest concentration spectrum presumable arising mostly from isolated Cu^{2+} ions, and the highest concentration spectrum presumably arising mostly from interacting pairs of Cu^{2+} ions. The spectrum of samples with intermediate concentrations appear to consist of a superposition of lines from both the isolated and interacting pair systems. Both nuclear isotopes, ^{63}Cu and ^{65}Cu have spin 3/2, magnetic moments +2.221 and +2.380 nuclear magnetons and are 69.1 and 30.9 percent naturally abundant, respectively.[5] Since their nuclear magnetic moments are approximately the same, it is impossible in the powder spectrum to separate

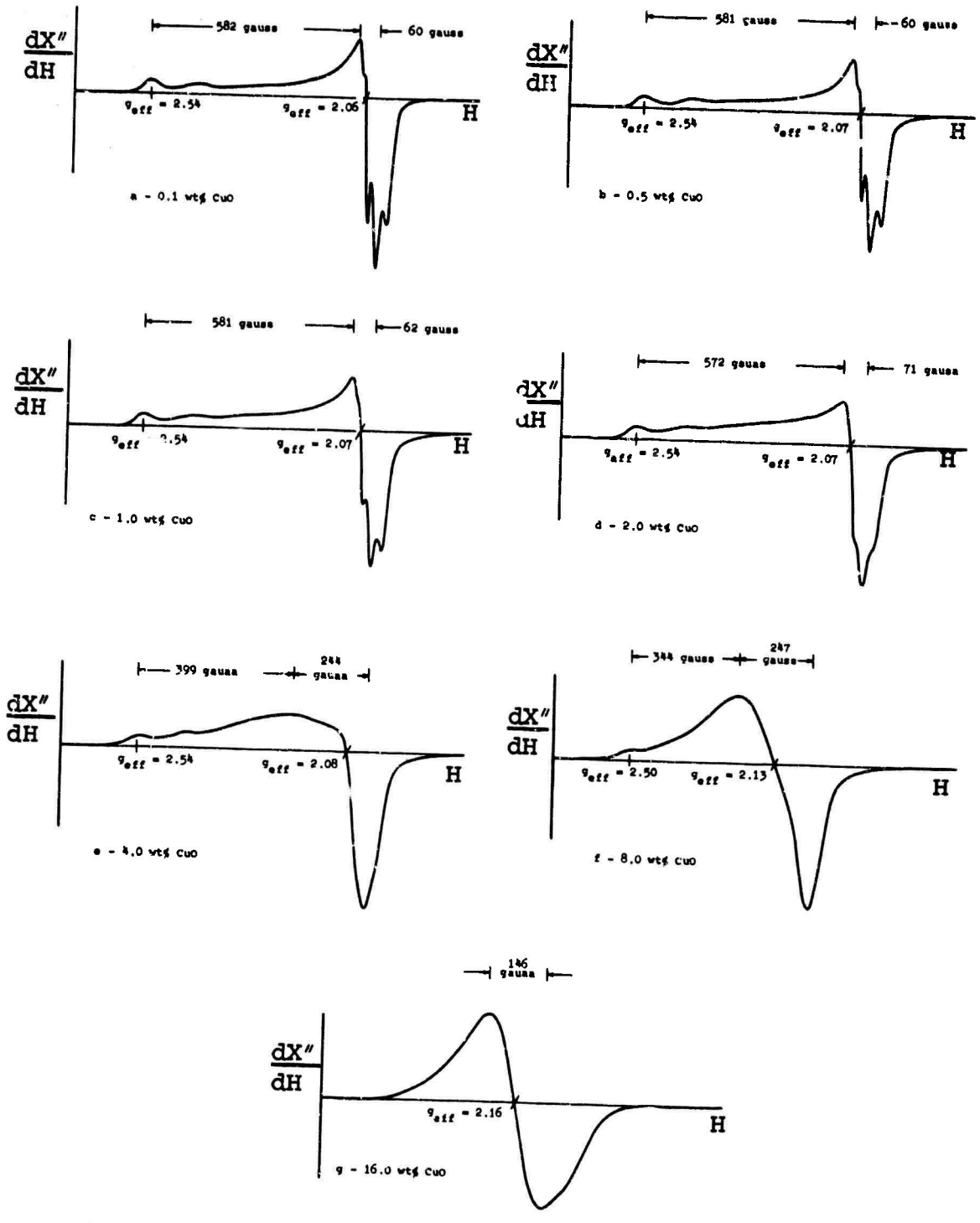

Figure 10. Concentration dependence of 9.4 kMc/sec ESR spectra of Cu^{2+} in a silicate glass doped with: a - 0.1 wt%; b - 0.5 wt%; c - 1.0 wt%; d - 2.0 wt%; e - 4.0 wt%; f - 8.0 wt%; and g - 16.0 wt% CuO at 77°K.

the hyperfine structure resulting from each. Thus, for analysis of the powder spectrum, all of the Cu^{2+} ions will be considered to have nuclear spin of 3/2 with the same magnetic moment.

The spectrum shown in Fig. 10a for isolated Cu^{2+} ions was interpreted in terms of the spin Hamiltonian for a system with axial symmetry.[6]

$$H_s = g_{\parallel} \beta H_z S_z + g_{\perp} \beta (H_x S_x + H_y S_y) + A_{\parallel} I_z S_z + A_{\perp} (I_x S_x + I_y S_y), \quad (5)$$

Where β is the Bohr magneton, $g_{\parallel}$ and $g_{\perp}$ are the principal parallel and perpendicular components of the g tensor, $A_{\parallel}$ and $A_{\perp}$ are the principal parallel and perpendicular components of the hyperfine-coupling tensor; H_x, H_y, H_z are the components of DC magnetic field along the principal axes, and S_x, S_y, S_z, and I_x, I_y, I_z are the components of the electronic and the nuclear spin angular momentum operators along the principal axes, respectively. It should be observed that since Cu^{2+} has S = 1/2, no fine structure terms appear in H_s.

In a single crystal doped with Cu^{2+}, the spectrum for a given orientation of the DC magnetic field should consist of a single absorption line split up into four hyperfine components. The line position in magnetic field units of the hyperfine components to second order is given by

$$H(m) = \frac{h\nu_o}{\beta g} - \frac{1}{\beta g}\left[Km - \frac{A_{\perp}^2}{4h\nu_o}\right]\left[\frac{A^2 + K^2}{K^2}\right]\left[I(I+1) - m^2\right], \quad (6)$$

where $g = (g_{\parallel}^2 \cos^2\theta + g_{\perp}^2 \sin^2\theta)$

and $K^2g^2 = A_{\parallel}^2 g_{\parallel}^2 \cos^2\theta + A^2 g^2 \sin^2\theta$,

where θ is the angle between the DC magnetic field and the crytalline-field Z axis, m is the nuclear magnetic quantum number ($m = \pm 3/2, \pm 1/2$), and I is the total nuclear magnetic quantum number. In the powder spectrum of Fig. 11a, the low field portion of the spectrum shows the poorly resolved hyperfine structure(hfs) pattern corresponding to the $\theta = 0$ parallel orientation, while the high-field portion shows a strong absorption consisting of

partially resolved hfs corresponding to the $\theta = \pi/2$ orientation. Calculation of the g- values and hyperfine coupling parameters are based on the line positions of the hyperfine transitions. Analysis of the spectrum of the sample containing 0.1 wt. % CuO gives the parameters;

$g_{\parallel} = 2.335 \pm 0.002$ $\quad |A_{\parallel}| = 155 \pm 1 \times 10^{-4}$ cm^{-1}

$g_{\perp} = 2.050 \pm 0.001$ $\quad |A_{\perp}| = 22.7 \pm 0.1 \times 10^{-4}$ cm^{-1}

An electron spin resonance and optical absorption study of Cu^{2+} in amorphous and polycrystalline GeO_2 and optical absorption studies of Cu^{2+} in silicate glass showed that Cu^{2+} is octahedrally coordinated in glass in a cubic crystal field with a large tetragonal distortion.[9,10] These conclusions have been confirmed in this study. Further experiments are planned which may allow for the construction of reasonable models of the local environment of isolated Cu^{2+} ions in glass.

From Fig. 10 (b-g), it can be seen that the two systems of lines which arise from isolated Cu^{2+} and interacting pairs of Cu^{2+} ions both occur in the same region of magnetic field at 9.49 kMc/sec. As for Mo^{5+}, the changes in the spectra may be due to a dipolar broadening mechanism or to the more subtle exchange interaction. As before, if the changes are due to an exchange interaction, it may be possible to separate the spectra of the two systems by performing additional ESR experiments at different frequencies. Other studies which may be helpful in elucidating the nature of the changes include computer lineshape analysis and termperature dependent intensity studies of the ESR spectrum.

3. EXPERIMENTAL INVESTIGATIONS OF COLOR CENTERS DEFECTS IN LASER GLASS

3.1 INTRODUCTION

Two types of color center defects are produced in certain laser glasses when pumped with ultraviolet light.[11] These are permanent and relatively short lived color centers. The permanent centers are characterized by permanent absorption bands in the visible and in the ultraviolet. The short lived centers are characterized by a saturable absorption at the Nd^{3+} laser wavelength which gives rise to limit cycle and Q-switching behavior. To date, investigations have been primarily concerned with a better characterization of their optical absorption and activation spectra, and are described below.

3.2 PERMANENT COLOR CENTER DEFECTS IN GLASS

The transmission spectrum of a 2 mm thick sample of a laser base glass which had been solarized by ultraviolet irradiation from a Xenon flashtube is shown in Fig. 11a. For purposes of comparison, the transmission spectrum of a 2 mm thick sample of the same clear base glass is shown in Fig. 11b. The base glass consists of 68% $Si\,O_2$, 16.5% K_2O, 8.0% Na_2O, 5.0% Ba O, 1.5% Al_2O_3 and 1.0% Li_2O, all in wt. % of the oxides. All starting materials were of reagent grade. The optical absorption spectrum of the colored glass is shown in Fig. 12. In this figure is plotted $\log_{10} T_2/T_1$ vs. wavelength λ, where T_1 and T_2 are the transmission of the solarized and unsolarized samples shown in Fig. 11, respectively. The three absorption bands which are centered about 250 nm, 450 nm, and 620 nm are similar to absorption bands obtained by Kats and Stevels in a ultraviolet solarized silicate glass.[12]

Kats and Stevels have determined that glasses can be colored by ultraviolet irradiation in the region of 250 nm.[12] In this study, experiments have been successfully performed which allow for a more precise determination of the activation spectrum for color center production. A one mm thick plate of the above laser base glass was irradiated by a 500 watt Xenon lamp for seven hours in the exit plane of a quartz crystal prism spectrograph as shown in Fig. 13. The dispersion curve of the spectrograph is shown in Fig. 14 in order to show the deviation obtained. In this experiment, since the glass is colored selectively as a function of wavelength, the density profile of color centers as a function of wavelength can be easily determined by the use of a microdensitometer with appropriate filters. The photocell in the microdensitometer measures the intensity of the transmitted light through the colored plate. The ratio of the

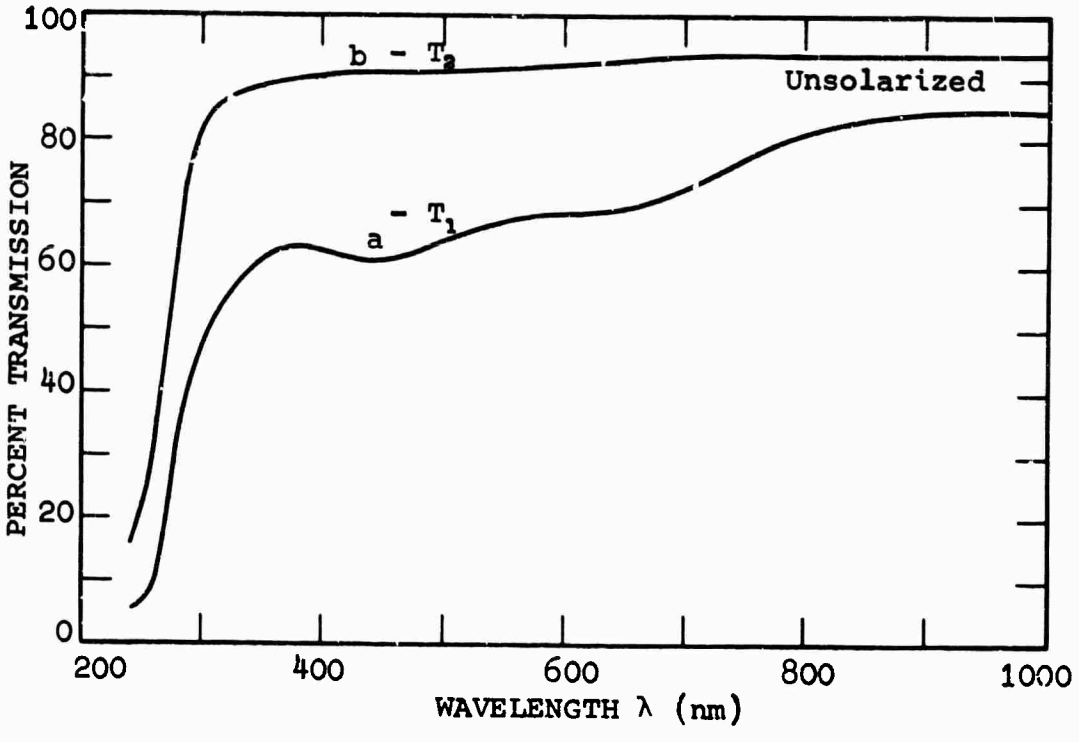

Fig. 11. Optical transmission spectra of 2 mm thick laser base glass of composition 68 wt. % SiO_2, 16.5 wt. % K_2O, 8 wt. % Na_2O, 5 wt. % BaO, 1.5 wt. % Al_2O_3, and 1.0 wt. % Li_2O; a, solarized by ultraviolet light from Xenon flashtube and b, unsolarized.

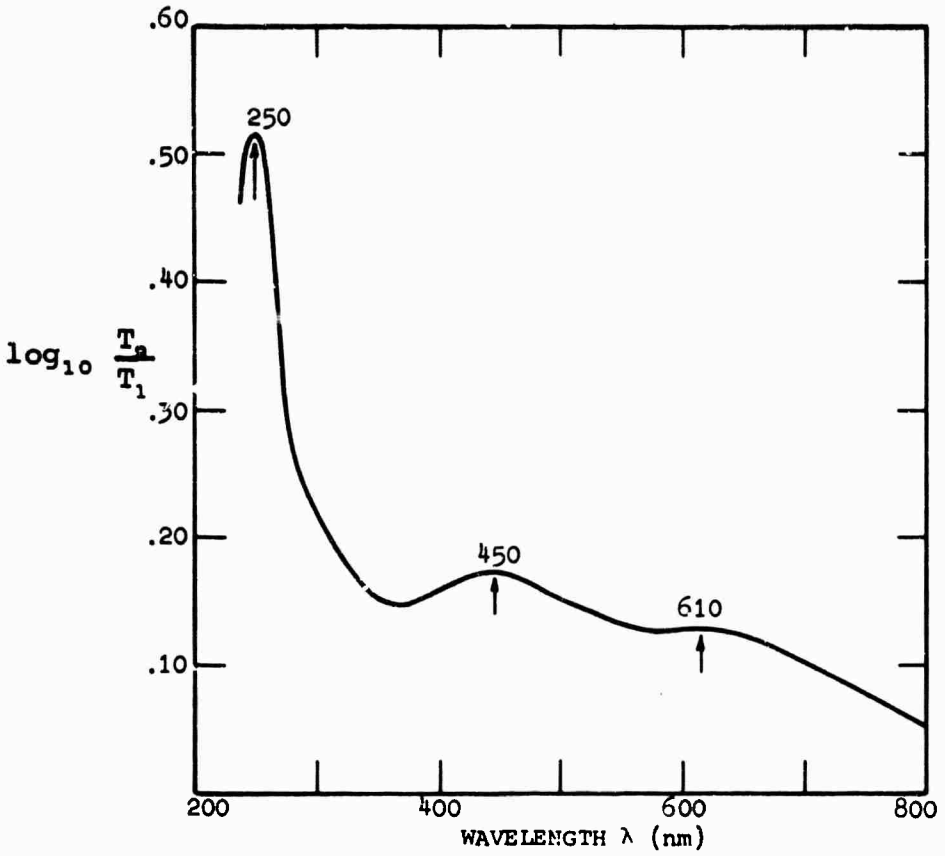

Fig. 12. Optical absorption spectrum of solarized laser base glass. T_1 and T_2 are the transmission of the solarized and unsolarized samples shown in Fig. 12, respectively.

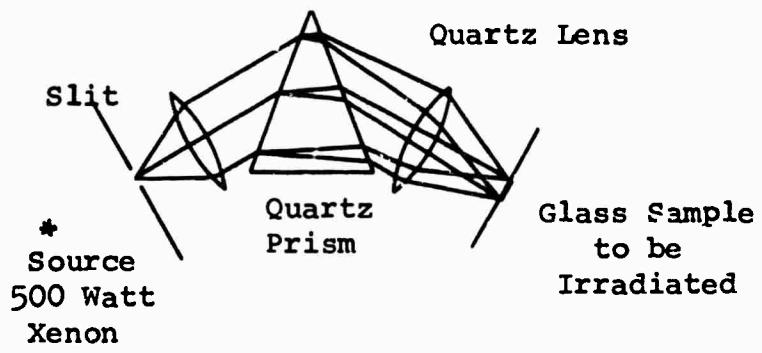

Fig. 13. Diagram of experimental set up used to determine the activation spectrum for production of permanent color center defects in the laser base glass.

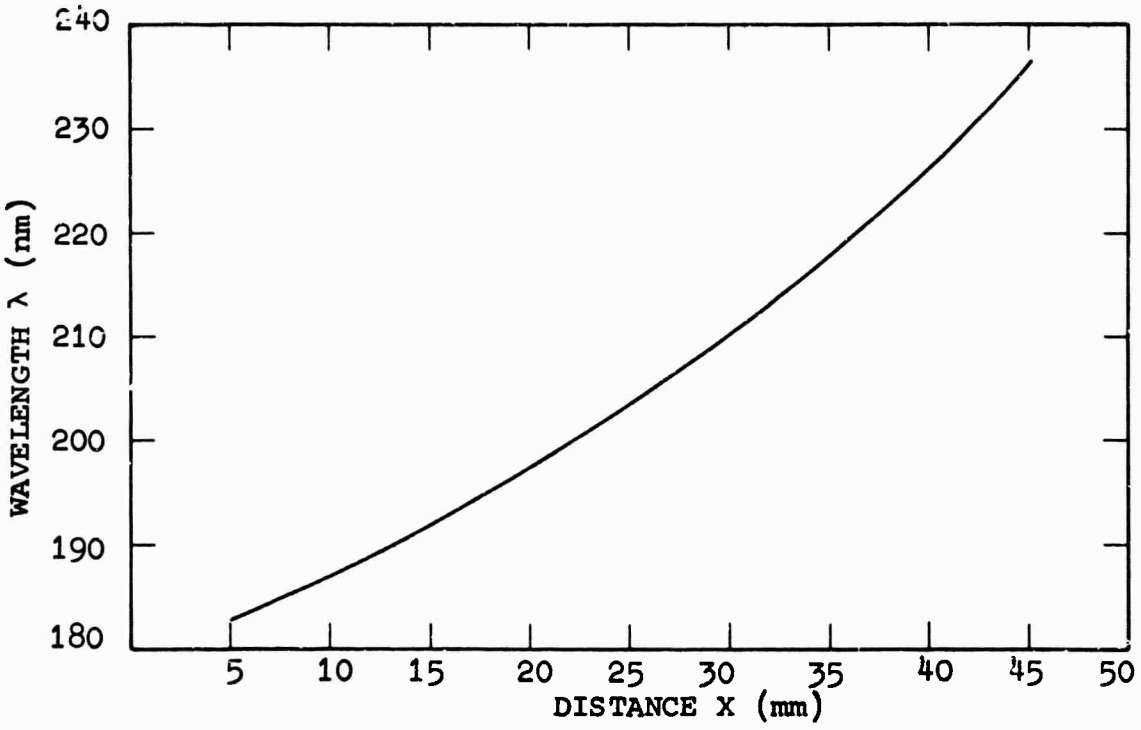

Fig. 14. Dispersion curve of the Hilger and Watt quartz prism spectrograph used to determine the activation spectrum for production of permanent color center defects in the laser base glass.

light transmitted through the plate to the incident light is given by

$$\frac{I}{I_o} = \frac{\int_{\lambda_1}^{\lambda_2} I(\lambda) 10^{-\alpha(\lambda)N} d\lambda}{\int_{\lambda_1}^{\lambda_2} I(\lambda)\, d\lambda} \qquad (7)$$

where $I(\lambda)$ is the intensity of the light at wavelength λ, $\alpha(\lambda)$ is the extinction coefficient of the absorber at wavelength λ, and N is the number of absorbers. For the color centers in this base glass, it can be seen from Fig. 11, that $\alpha(\lambda)$ in the visible region is a very slowly varying function of wavelength. Thus, in analysing the density profiles using fairly sharp yellow and blue light glass filters, $\alpha(\lambda)$ in eq. (9) can be considered to be constant. In this approximation, the number of color centers is given by $1/\alpha \log_{10} I_o/I$. Microdensitometer density profiles of the colored glass plate were obtained using yellow and blue filters, which allowed for selective absorption in the 620 nm and 450 nm bands, respectively. Since the density profiles obtained in this manner were very nearly identical, only the profile obtained with the yellow filter is shown in Fig. 15. In Fig. 15a is plotted the relative number of color centers produced as a function of activation wavelength λ. It can be seen from Fig. 15a that the maximum number of color centers in this glass are produced by photons having wavelength $\lambda \cong 216$ nm and that the activation wavelength full width at half maximum is a fairly narrow 13 nm. The dispersion curve of the quartz prism spectrograph was calibrated by using the line spectra of a 100 watt low pressure mercury arc lamp.

In order to determine the activation spectrum for color center production which is independent of the irradiation source, the relative output intensity of the 500 watt Xenon lamp in the wavelength region 200-260 nm was obtained. In order to accomplish this, a 1 mm thick soft clear glass plate was uniformly coated with a 0.5M solution of sodium salicylate in methyl alcohol to a thickness of 1 mg/cm^2 by an artist's air brush. Sodium salicylate was chosen since it fluoresces in the blue with constant fluorescence quantum yield over a wavelength range from approximately 60 to 340 nm with an efficiency which approaches unity for suitably prepared layers.[13] This plate was irradiated in the exit plane of the quartz prism spectrograph by the 500 watt Xenon lamp, and the relative fluorescent intensity as a function of irradiation

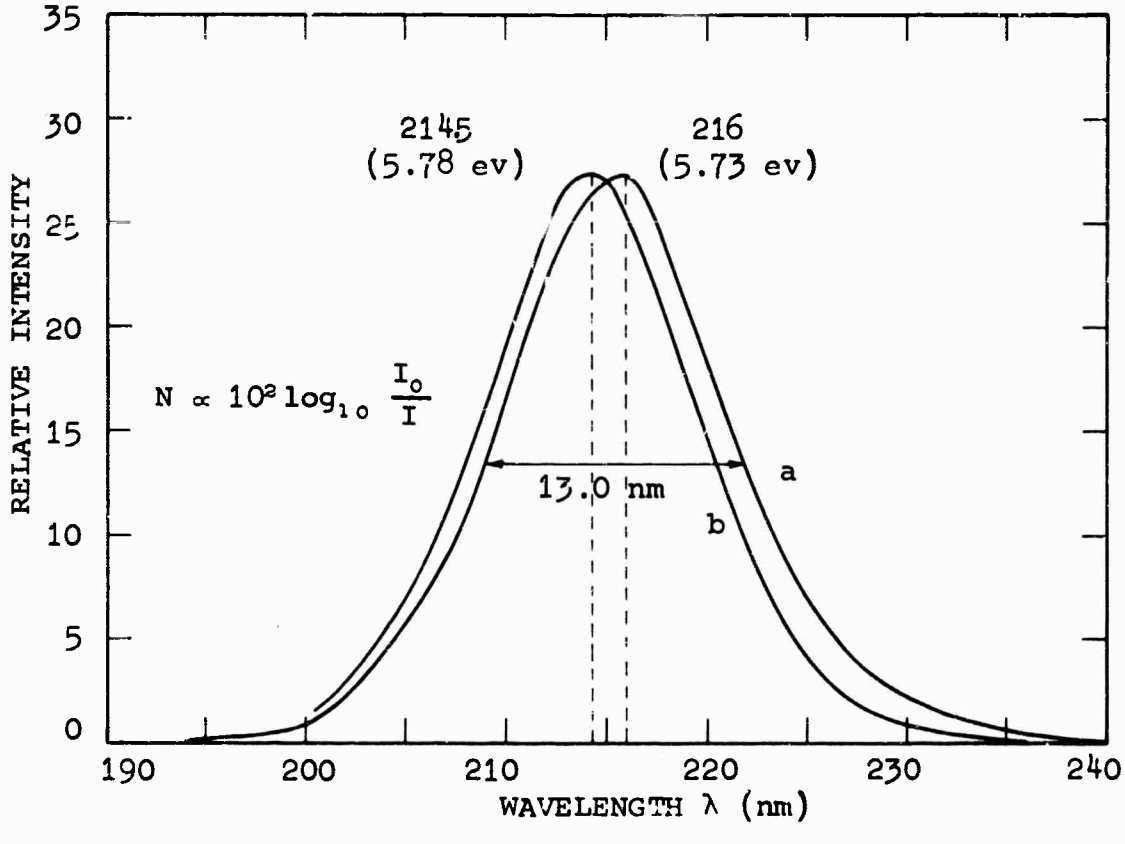

Fig. 15. Activation spectra for production of permanent color center defects in the laser base glass when irradiated for seven hours at 300°K with a 500 watt Xenon lamp; (a) source dependent; and (b) normalized and approximately source independent.

wavelength was measured through a 1/2 mm slit by a type 5H surface photocell. Over the intensity region of interest, the response of the photocell is linear. The resulting relative output intensity $I(\lambda)$ of the lamp as a function of wavelength λ is shown in Fig. 16. The number of photons of wavelength λ per unit area per unit time is given by

$$N_\lambda = \frac{I(\lambda)}{h\nu_\lambda}$$

Thus, it is possible to obtain the relative activation spectrum for permanent color center production in this glass approximately independent of the source used by taking the ratio of the number of color centers produced to the number of incident photons at wavelength λ. When this is done, the curve shown in Fig. 15b results. The net effect on the activation spectrum is to shift the entire curve to shorter wavelengths and higher energies as expected. Thus, the activation spectrum for color center production in this glass now occurs at $\lambda \cong 214$ nm or 5.78 ev. The line width appears to remain essentially unchanged. Since the saturation value of the optical density as a function of irradiation wavelength has not been studied, and since the sample was irradiated for a period of seven hours, the curves in Fig. 15 may contain some saturation effects. In order to clarify this point, a study of the activation spectrum as a function of irradiation time will be undertaken.

It should be emphasized that the curve shown in Fig. 15b for the activation spectrum is a good approximation only, since the relative intensity of the ultraviolet light from the lamp was not recorded while the glass was being irradiated but was recorded immediately following the irradiation. The importance of this experiment at this time is that a technique has been evolved which allows for a fairly precise determination of the activation spectrum for color center production in the solid state.

Plans for the future include obtaining the activation spectrum for the above glass containing in addition 5.0 wt. % Nd_2O_3. Further, since the effect of various alkali and alkaline earth metals on color center production in this glass are not very well understood, a systematic study of this glass containing various amounts of alkali and alkaline earth metals will be undertaken. The glasses, which are presently being fabricated, will be solarized, their optical spectra will be recorded and analyzed, and their activation spectra will be obtained. Hopefully, this study will lead to the fabrication of a more solarization resistant laser glass.

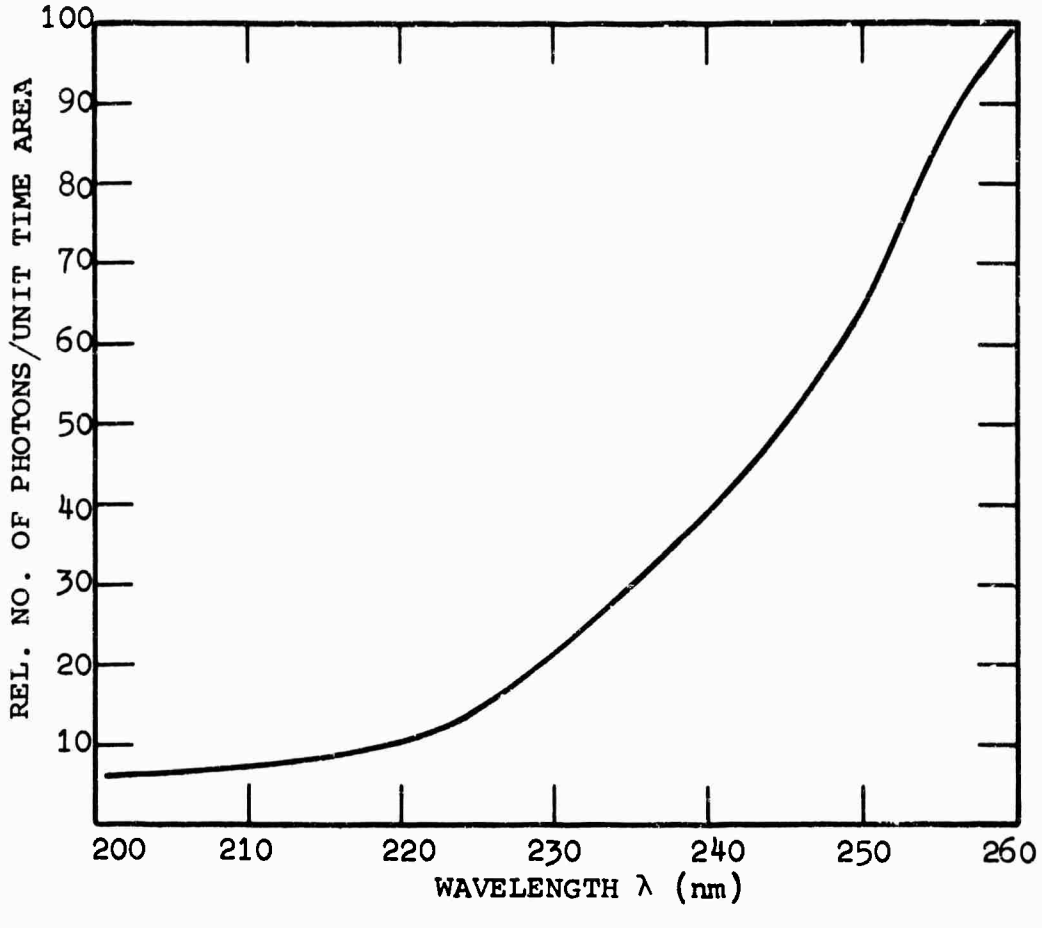

Fig. 16. Relative output intensity of 500 watt Xenon lamp. In this figure is plotted the relative number of photons per unit area time vs. wavelength λ in nm.

3.3 SHORT LIVED COLOR CENTER DEFECTS IN GLASS

Experiments were undertaken in an attempt to obtain the optical absorption spectrum of the short lived color center defect. The experiment basically consists of monitoring the transmission of light from a monochromator through polished ends of a rod of the above laser base glass while the rod is simultaneously pumped from the sides with light from two Xenon flashtubes. To date, the results contain such a large amount of scatter that it is not possible to obtain a meaningful optical absorption spectrum. Modifications of the above experiment are presently underway in an attempt to determine if it is possible to reduce the experimental scatter to the point where a meaningful absorption curve may be obtained. All that can be said at this time is that the absorption spectrum of the short lived color center defect may have some structure. Greater detail of the apparatus and experimental effort will be contained in a later report. Using this same apparatus, future plans will include attempts to obtain a more precise value of the lifetime of these short lived color center defects. These experiments will involve monitoring the increase of the transmission of the light through the glass rod immediately following excitation by Xenon flashtubes, the pulse shape of which will be made to be approximately square wave by use of appropriate LC circuits.

In a previous study, it was shown that ultraviolet light below 310 nm is required to produce the short lived color centers which give rise to limit cycle or Q-switching laser action due to the saturable absorption of these centers at the Nd^{3+} laser wavelength of 1.06u.[11] In this work, experiments were undertaken in an attempt to more precisely determine their activation spectrum. Laser experiments were performed using various liquid filters with fairly sharp cut-offs in the ultraviolet region in order to determine the upper bound of the activation spectrum. A diagram of the experimental arrangement is shown in Fig. 17. The experimental laser cavity configuration consists of a 40.6 cm long 4 mm diameter Nd^{3+} doped laser rod surrounded by Pyrex tubing and close wrapped with silver foil to a 25.4 cm Xenon flashtube in a water cooled cavity. Twelve and one half centimeters of the laser rod protruded beyond the water filled cavity. Nine centimeters of this section of the laser rod was close-wrapped with silver foil to a 12.5 cm long 15 mm ID quartz tube which contained the liquid filter and an 8.9 cm Xenon flashtube as shown in Fig. 17. In addition, a baffle was placed between the flashtube and the laser rod so that all the light from the 8.9 cm flashtube which reached the laser rod had to traverse the liquid filter. The rod contained a polished flat on one end and a 45° roof at the other, thus providing a 4%

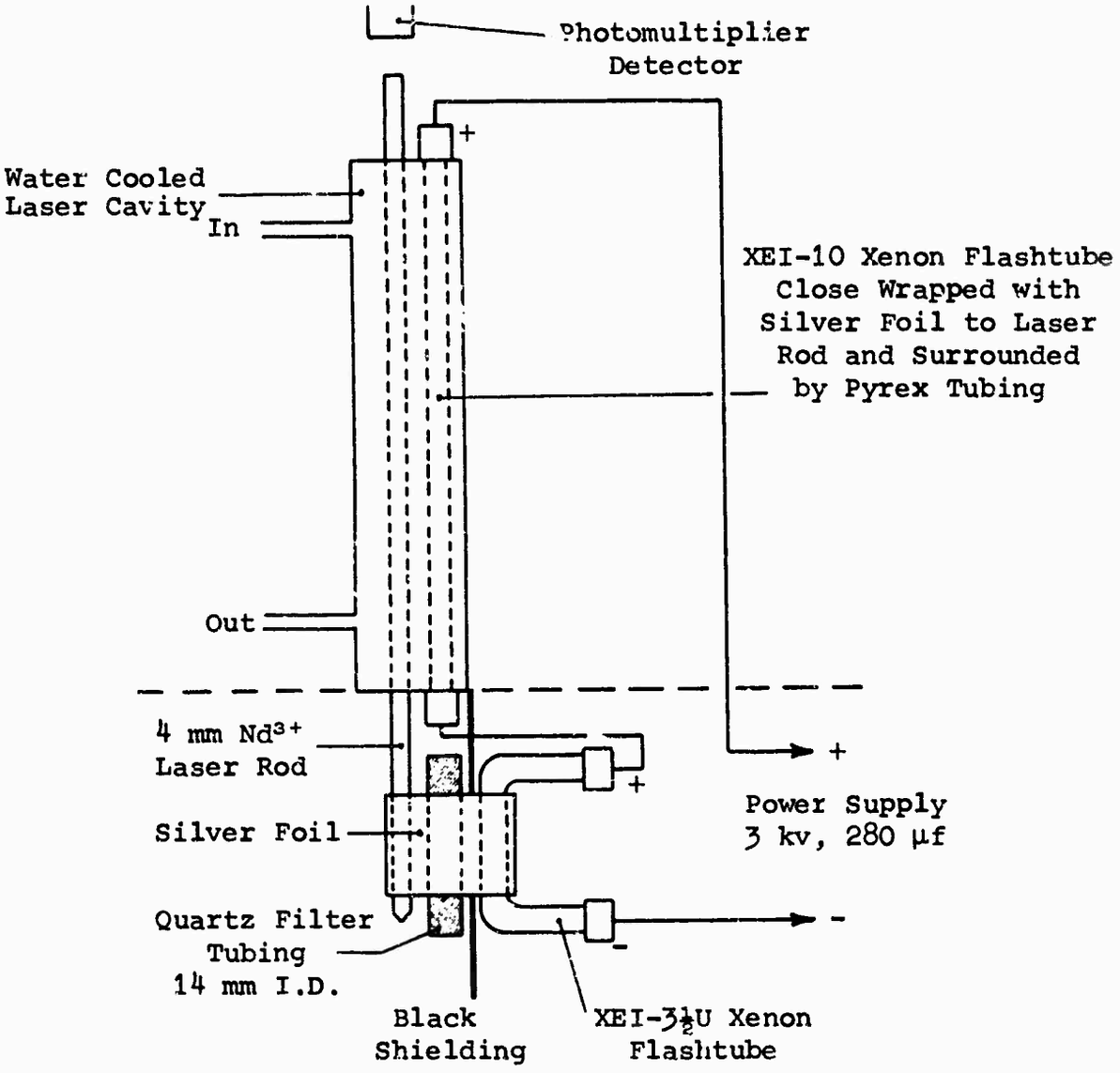

Fig. 17. Experimental liquid filter laser configuration used to determine the upper bound of the activation spectrum for production of short lived Q-switching color center defects.

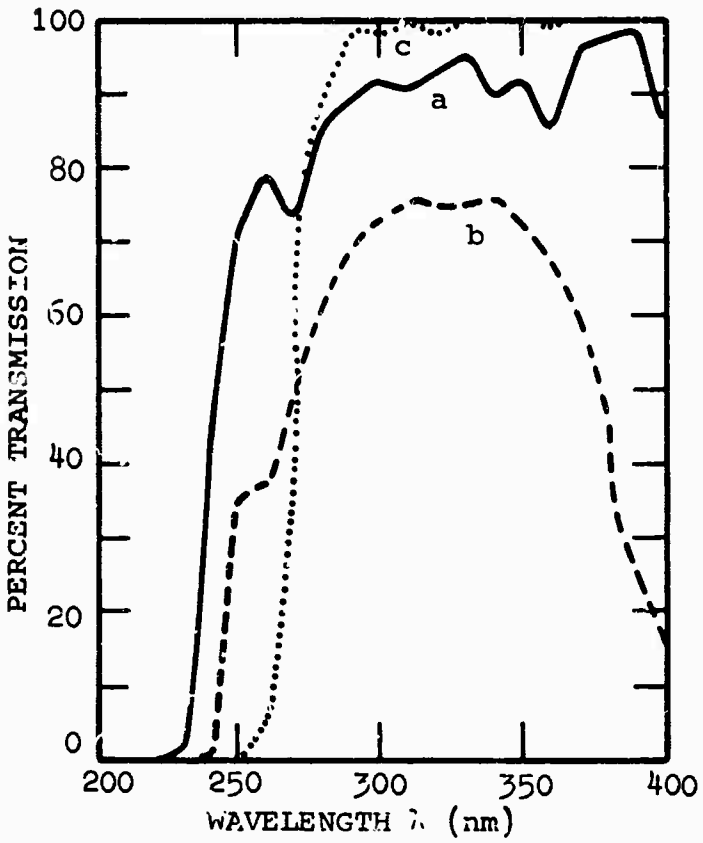

Fig. 18. Transmission spectra of 1 cm thick liquid filter referenced to water showing transmission cut-offs in the ultraviolet region for: (a) 500 g/l aqueous solution of $MnCl_2$; (b) 500 g/l aqueous solution of $CoCl_2$; and (c) CCl_4.

reflectance at the glass flat air interface and 98% reflectance at the roof end. The two flashtubes were connected in series, and the power supply was operated at 3.2 KV with a capacitance of 280 microfarads and an inductance of 58.4 microhenrys. Thus, approximately 1000 joules were dissipated across the 25.4 cm flashtube and approximately 400 joules were dissipated across the 8.9 cm flashtube. The liquid filters chosen were carbon tetrachloride (CCl_4), maganese chloride ($MnCl_2$), and cobalt chloride ($CoCl_2$). The transmission spectra of 1 cm thick liquid samples of the above liquids referenced to distilled water are shown in Fig. 18. Previous results showed that quartz filters allowed for production of the color centers and that Pyrex filters prevented their creation.[11] Hence, it is only necessary to compare the laser behavior when pumped through the liquid filters to the behavior obtained when pumping through Pyrex and quartz tubing containing distilled water. Oscilloscope traces of the laser behavior when pumping through the various filters are shown in Fig. 19. From Fig. 19, it can be seen that damped oscillations in the laser output are obtained when pumping through Pyrex, CCl_4, and $CoCl_2$, and that limit cycle behavior is obtained when pumping through $MnCl_2$ and quartz. Hence, it is possible to conclude from the above and from Fig. 18 that ultraviolet light below 240 nm is required to produce the short lived color center defect.

In place of pumping the laser rod through various liquid filters, attempts were made to pump the exposed end of the laser rod shown in Fig. 17 through the quartz prism spectrograph which was used to determine the activation spectrum of the permanent color center defect. The numerical aperture (N. A.) of the system was not large enough to produce a detectable number of short lived color center defects. Attempts to devise a larger N. A. system are presently underway.

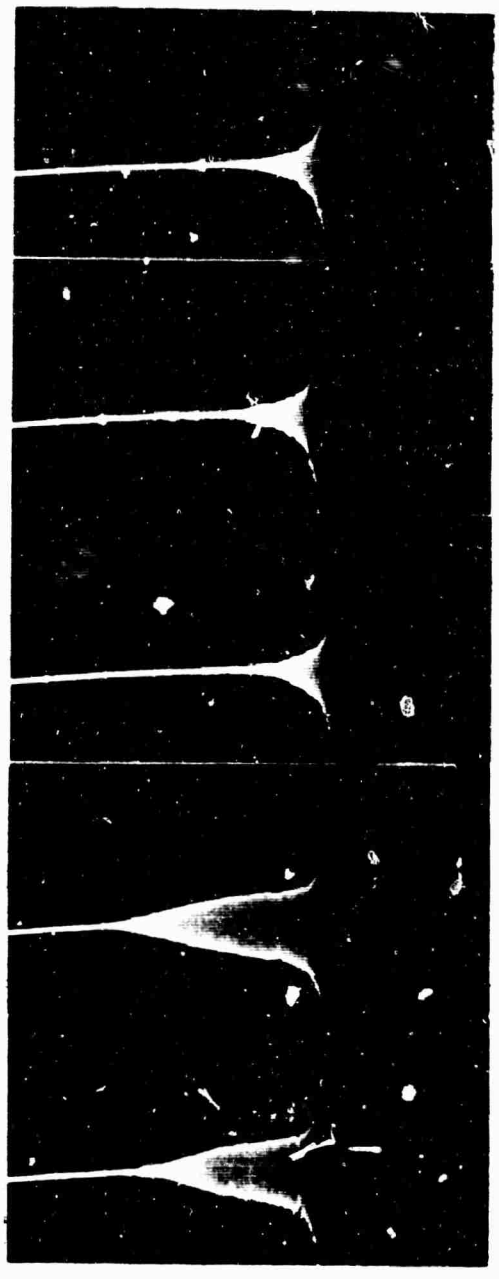

Fig. 19. Laser time traces obtained when pumping through the liquid filters: (a) water in Pyrex tubing; (b) CCl_4 in quartz tubing; (c) $CoCl_2$ in quartz tubing; (d) $MnCl_2$ in quartz tubing; (e) water in quartz tubing. The Pyrex and quartz tubing were 15 mm in diameter and had wall thicknesses of 1 mm. The time traces were taken with a sweep speed of 50 μsec/cm. Increasing time is from right to left.

4. THEORETICAL INVESTIGATIONS OF VITREOUS MATERI

4.1 INTRODUCTION - COLO CENTERS AND GLASS STRUCTURE

A number of investigators studying optical and ESR spectra of irradiated glasses of diverse composition have suggested that holes trapped on network-forming polyhedral units constitute an important source of color center absorption in glass.[14,15,16,17] As a specific example, it has long been known that the silicon-oxygen tetrahedron is a basic structural unit of vitreous SiO_2.[18] The glass network is thought to be composed of linked tetrahedra sharing a common bridging oxygen. In the presence of alkali or alkaline earth ions, some of the oxygens become non-bridging in the sense that they are not common to two tetrahedra. Schreurs has proposed color center models consisting of a hole trapped on silicon-oxygen tetrahedra with two or three non-bridging oxygens.[17] Trapped hole centers associated with network forming tetrahedra in borate and phosphate glasses have also been suggested.[14,15,16]

Though these tetrahedral complexes in glass are of obvious importance, no detailed theoretical study of their electronic structure has been reported. The reason for this no doubt lies in the fact that the quantum mechanical calculation of the structure of large polyatomic molecules is a laborious task. However, given present day computer programs for evaluating difficult multicenter integrals, it seems feasible to undertake a theoretical study of these complexes.

4.2 MOLECULAR THEORY - QUALITATIVE

Two theoretical approaches are commonly employed in the description of molecular electronic structure. In the molecular orbital (MO) approach, one constructs delocalized orbitals which are labeled by irreducible representations of the molecular point group symmetry. Selection rules, transition moments, and the polarization of optical absorptions are conveniently described in this model.

In cases where the molecular structure indicates strong directional tendencies for bonding of a particular species, the valence bond approach provides a more transparent picture of electronic structure. Localized orbitals directed along interatomic axes are constructed and utilized in calculation of molecular electronic properties. This picture of electrons concentrated in directed bonds correlates well with intuitive ideas of chemical bonding, and if the method is applied rigorously, quite good values of bond energies and bond angles can be obtained. Furthermore,

localization of electrons makes possible a separation of local and distant effects to a much greater degree than is possible in the MO picture. In view of these factors, the valence bond approach seems well suited to a study of the tetrahedral network formers in glass.

4.3 THE SILICON-OXYGEN TETRAHEDRON WITH ONE NON-BRIDGING OXYGEN

The silicon-oxygen tetrahedron with one non-bridging oxygen has been chosen as the initial subject for investigation. It is felt that by concentrating attention on the non-bridging oxygen, a tractable program of calculation can be established which will provide insight into the electronic structure of the tetrahedral units and of the associated color centers. To define the problem, and to point to some anticipated results, it is helpful to consider the tetrahedral bonding qualitatively. First, it is necessary to distinguish in a fundamental way a bridging from a non-bridging oxygen. In the case of a tetrahedron with all oxygens bridging, the bonding is reasonably described in the following manner. Tetrahedrally directed sp^3 hybrids can be prepared from Si 3s and 3p atomic orbitals. These tetrahedral hybrids overlap appropriate orbitals on the oxygens and form σ bonds. If Si-O-Si bond angles of 180° are assumed, the appropriate oxygen orbitals are sp hybrids. The remainder of the oxygen electrons occupy atomic oxygen 2p orbitals perpendicular to the Si-O-Si bond direction. In fact, the Si-O-Si bond angle in silicate glass varies over a wide range with an average in the vicinity of 153°. Consequently, the choice of oxygen sp hybrids corresponds to an extreme case. Since we concentrate on the non-bridging oxygen, the exact state of hybridization of the bridging oxygen is not of primary concern, and will not be given detailed consideration in the first order treatment of the tetrahedron.

In the case of a non-bridging oxygen additional electronic charge is associated with the oxygen, and a lone pair of electrons occupying a lobe of the sp hybrid results. The increased inter-electronic repulsion due to the concentration of charge at the oxygen site makes it likely that the energy of the complex would be reduced by a shift of oxygen p electron charge onto the Si by means of π bonding. Since the π bonds involve high energy d and f atomic orbitals on the Si, it seems probable that a bridging oxygen, lacking the excess charge, would not exhibit any π bonding tendency. Consequently, it is proposed that those p electrons associate with a bridging oxygen which are not involved in formation of σ bonds be assigned to oxygen 2p atomic orbitals. In the case of a non-bridging oxygen, the analogous p electrons are assigned to π bonds.

The initial objective of this study is to establish a formal description of the π orbitals and to determine if a π bonding electron is, in fact, more stable than an atomic p electron associated with a non-bridging oxygen. This information will provide an indication of the extent to which π bonding can be effective in stabilizing excess charge at a non-bridging oxygen site, and will therefore help clarify the role of the network-modifying cations. Furtner, it is not apparent from a priori considerations whether the π electrons or the σ lone pair electrons have the lower energy. Since the creation of a color center presumably arises from the freeing of an electron associated with a non-bridging oxygen, the comparison between σ lone pair and π electron energies is of interest. Finally, the effect of nearby cations on σ and π energies is a worthwhile topic for investigation which can be undertaken as an extension of the present study.

4.4 FORMAL DISCUSSION OF VALENCE BOND THEORY

Consider a polyatomic molecule in the valence bond picture. Let the i^{th} bond be formed from spatially localized orbitals A_i and B_i . The electronic Hamiltonian for the molecular system in atomic units is

$$\mathcal{H} = \sum_i \left[-\nabla_i^2 - \sum_\alpha \frac{2Z_\alpha}{r_{i\alpha}} \right] + \sum_{\substack{i,j \\ i \neq j}} \frac{2}{r_{ij}} \qquad (8)$$

It has been shown by Hurley, Lennard-Jones, and Pople, that if the functions A_i and B_i are orthogonal to all orbitals associated with other bonds (A_i and B_i are <u>not</u> mutually orthogonal), then the average energy of the molecular system $\langle \mathcal{H} \rangle$ has a simple form.[19] The method has been discussed at length by Slater.[20]

Neglecting certain small terms, the energy expression is[20]

$$\langle \mathcal{H} \rangle = \sum_i (1 + S_i^2)^{-1} \Big\{ [A_i|A_i] + 2S_i [A_i|B_i] + [B_i|B_i] + [A_iA_i|B_iB_i] + [A_iB_i|B_iA_i] \Big\}$$
$$+ \sum_{\substack{i,j \\ i \neq j}} (1 + S_i^2)^{-1} (1 + S_j^2)^{-1} \Big\{ [A_iA_i|A_jA_j] + [A_iA_i|B_jB_j] + [B_iB_i|A_jA_j] + [B_iB_i|B_jB_j] + 2S_i \Big([A_iB_i|A_jA_j] + [B_iA_i|B_jB_j] \Big) + 2S_j [A_jB_j|A_iA_i] + [B_jA_j|B_iB_i] + 4S_iS_j [A_iB_i|A_jB_j] \Big\} \qquad (9)$$

Here S_i is the overlap integral

$$S_i = \int A_i B_i \, d\tau, \qquad (10)$$

and the remaining integrals are defined by the relations

$$[a|b] = \int a^*(1) \left[-\nabla^2 - \sum_\alpha \frac{2Z_\alpha}{r_{i\alpha}} \right] b(1) \, d\tau_1, \qquad (11)$$

and

$$[ab|cd] = \iint a^*(1) \, b(1) \, \frac{2}{r_{12}} \, c^*(2) \, d(2) \, d\tau_1 \, d\tau_2. \qquad (12)$$

The first sum in Eq. (9) represents a sum over bonds of the energy of each isolated bond. The second sum represents the electrostatic interaction between bonds. A third term representing small exchange interactions between charge distributions consisting of products of orthogonal functions is omitted.[21] Thus, the expression for the total energy has a simple interpretation in terms of individual bond energies and intra-bond interaction. It is this feature which makes the approach particularly useful if one wishes to focus attention on local interactions and to take into account the effects of distant ions in some approximate fashion.

If, for example, one were to compute the energy of an O-Si bond associated with a non-bridging oxygen, one could in a reasonable approximation treat explicitly only the electronic interaction of the bond under study with those bond functions associated with the non-bridging oxygen and the silicon, while reducing the three bridging oxygens to point ions. Such an approach has been successfully employed by Coulson, Redei, and Stocker[21] in studies of various tetrahedral intermetallic compounds, and will be used in the treatment of the Si-O tetrahedron.

It should be emphasized that if the energy expression is to take the simple form of Eq. (9), it is essential that the functions A_i and B_i be orthogonal to all A_j and B_j . In treating the σ bonding of the tetrahedral structure the orthogonality is attained to good approximation through the use of central ion sp^3 hybrids and ligand sp hybrids. In the presence of π bonding the situation becomes more complicated. Clearly, the orthogonality condition will not be satisfied if the π electrons occupy diffuse molecular orbitals which encompass the entire complex. A central feature of our approach to the π bonding in the silicon-oxygen tetrahedron is therefore the introduction of directed π bonding hybrids analogous to the familiar hybrids used in the description of the σ structure. Eight directed π hybrids which favorably overlap oxygen π orbitals are constructed from silicon atomic orbitals. These eight functions are mutually orthogonal and orthogonal to the tetrahedral sp^3 hybrids. The π bonding of the non-bridging oxygen is then accounted for by forming bonds from the p functions of the non-bridging oxygen and the two appropriate directed π hybrids. Those π hybrids concentrated in the direction of bridging oxygens are not occupied in the bond scheme.

4.5 THEORY OF DIRECTED π BONDS IN TETRAHEDRAL COMPLEXES

The procedure for determining the π hybrids is derived from the group theory. The essential features are described by van Vleck[22] in an early paper in which the group theoretic connection between the Mo and valence bond theories is discussed. It was mentioned earlier that in the MO description one utilizes orbitals which transform as bases for irreducible representations of the molecular point group. Directed bond functions, on the other hand, transform as reducible representations. In the case of a tetrahedral complex, the ligand p_x and p_y functions (the z

irreducible representations Γ_4 and Γ_5. It follows that central ion orbitals of all three symmetry types are required to construct valence hybrids transforming as the ligand p_x and p_y functions. Functions of Γ_3 and Γ_4 symmetry can be constructed from central ion d orbitals, but one must go to f orbitals to obtain functions of Γ_5 symmetry.

The connection between the directed hybrid orbitals and those atomic orbitals transforming as irreducible representations of the group T_d is made through the unitary matrix which reduces the representation spanned by the ligand p_x and p_y functions. Let the vector $\underset{\sim}{\Psi}$ be defined by the relation

$$\underset{\sim}{\Psi} = \begin{pmatrix} \psi_1 \\ \psi_2 \\ \vdots \\ \vdots \\ \psi_8 \end{pmatrix}, \tag{13}$$

where the ψ_j are the eight ligand p_x and p_y functions taken in some arbitrary order. These functions span a reducible representation Γ' of T_d which can be brought to reduced form by a unitary transformation defined by the matrix equation

$$\underset{\sim}{U}\underset{\sim}{\Gamma'}\underset{\sim}{U}^{\dagger} = \underset{\sim}{\Gamma} = \begin{pmatrix} \underset{\sim}{\Gamma}_3^* & & \\ & \underset{\sim}{\Gamma}_4^* & \\ & & \underset{\sim}{\Gamma}_5^* \end{pmatrix}. \tag{14}$$

Here $(\dagger)$ denotes adjoint, and for convenience in later manipulation the complex conjugates of the irreducible representations appear in the reduced representation matrix $\underset{\sim}{\Gamma}$. The functions ϕ defined by the matrix equation

$$\underset{\sim}{\phi} = \underset{\sim}{U}\,\underset{\sim}{\Psi} \tag{15}$$

constitute a basis for $\underset{\sim}{\Gamma}$. Conversely, if central ion functions $\underset{\sim}{\chi}$ form a basis for $\underset{\sim}{\Gamma}$, then the functions ξ_i defined by

$$\underset{\sim}{\xi} = \underset{\sim}{U}^{\dagger}\underset{\sim}{\chi} \tag{16}$$

are the desired directed π hybrids.

A prescription for evaluating the matrix U has been given by Koester.[23] Matrix elements U_{ij} are obtained from the relationship

$$\frac{n_\gamma}{g} \sum_{(R)} \Gamma'(R)_{ij} \Gamma_\alpha (R)_{kl} = U_{ki}^* U_{lj}, \qquad (17)$$

where n_γ is the dimension of the irreducible representation $\Gamma\alpha$ and Γ' is the reducible representation under consideration. The integer g is the order of the group (24 for T_d), and the sum extends over all elements R of the group. From this expression, it is seen that matrices for both irreducible and reducible representations are required. Irreducible matrices are given by Slater,[24] but matrices for the reducible representation spanned by the ligand functions must be evaluated. Note that by fixing l and j in Eq. (17) all elements of U can be obtained if only one column of each of the twenty four 8x8 reducible matrices is known. The necessary matrix elements of Γ' are obtained from the expression

$$R\,\psi_j = \sum_{n=1} \Gamma'(R)_{nj}\, \psi_n. \qquad (18)$$

If Slater's matrices are to be used, then the elements Γ'_{nj} must be determined in a compatible manner. To this end, Slater's defining relation[25]

$$R\psi(\vec{r}) = \psi(R\vec{r}) \qquad (19)$$

has been used to describe the effect of R on the basis function ψ. A compatible coordinate system is shown in Fig. 20. The central ion is located at the center of the cube. Ligand centered coordinates have their origins at corners a, b, c, and d with positive z axis directed toward the central ion. Direction cosines of th.. ligand axes at center "a" are:

$$\begin{aligned} x_a &: \left(+\sqrt{1/6}, -\sqrt{2/3}, -\sqrt{1/6} \right) \\ y_a &: \left(\sqrt{1/2}, 0, -\sqrt{1/2} \right) \\ z_a &: \left(-\sqrt{1/3}, -\sqrt{1/3}, -\sqrt{1/3} \right) \end{aligned} \qquad (20)$$

Coordinate systems at the other ligand centers are obtained by two-fold rotations about the central ion x, y, and z axes.

In evaluating Γ', the complex functions proportional to Y_1^1, and Y_1^{-1} are used instead of the real functions p_x and p_y. The previously defined vector Ψ is given by the relation

$$\underset{\sim}{\Psi} = f(r) \begin{pmatrix} Y_1^1 & (a) \\ Y_1^1 & (b) \\ Y_1^1 & (c) \\ Y_1^1 & (d) \\ Y_1^{-1} & (a) \\ Y_1^{-1} & (b) \\ Y_1^{-1} & (c) \\ Y_1^{-1} & (d) \end{pmatrix} \equiv \begin{pmatrix} \psi_1 \\ \psi_2 \\ \psi_3 \\ . \\ . \\ . \\ . \\ \psi_8 \end{pmatrix} \tag{21}$$

Since the details of the extensive analysis needed to evaluate the Γ'_{nj} from the defining relation Eq. (19), and to evaluate the matrix U from Eq. (17) would add little to the discussion, it is omitted. The resulting expression for $\underset{\sim}{U}$ is

$$\underset{\sim}{U} = \sqrt{8} \begin{pmatrix} 1 & 1 & 1 & 1 & \alpha & \alpha & \alpha & \alpha \\ -i & -i & -i & -i & \beta^* & \beta^* & \beta^* & \beta^* \\ 1 & 1 & -1 & -1 & \alpha & \alpha & -\alpha & -\alpha \\ \alpha^* & -\alpha^* & \alpha^* & -\alpha^* & \alpha^* & -\alpha^* & \alpha^* & -\alpha^* \\ \alpha & -\alpha & -\alpha & \alpha & 1 & -1 & -1 & 1 \\ 1 & 1 & -1 & -1 & -\alpha & -\alpha & \alpha & \alpha \\ \alpha^* & -\alpha^* & \alpha^* & -\alpha^* & -\alpha^* & \alpha^* & -\alpha^* & \alpha^* \\ \alpha & -\alpha & -\alpha & \alpha & -1 & 1 & 1 & -1 \end{pmatrix} \tag{22}$$

where

$$\begin{aligned} \alpha &= \exp(i\, 2\pi/3) \\ \beta &= \exp(-i\, 5\pi/6) \\ i &= \sqrt{-1}. \end{aligned} \tag{23}$$

The central ion bases functions are given by the relations

$$\chi_1 = g(r)\,\frac{1}{\sqrt{2}}\left[\sqrt{3/2}\,(Y_2^{2} + Y_2^{-2}) - Y_2^{0}\right]$$

$$\chi_2 = g(r)\,\frac{1}{\sqrt{2}}\left[-\frac{1}{\sqrt{2}}\,(Y_2^{2} - 1\,Y_2^{-2}) - \sqrt{3}\,Y_2^{0}\right]$$

$$\chi_3 = g(r)\,\frac{i}{\sqrt{2}}\,(Y_2^{1} + Y_2^{-1})$$

$$\chi_4 = g(r)\left(-\frac{i}{\sqrt{2}}\right)(Y_2^{1} - Y_2^{-1})$$

$$\chi_5 = g(r)\left(\frac{i}{\sqrt{2}}\right)(Y_2^{2} - Y_2^{-2}) \qquad (24)$$

$$\chi_6 = R(r)\,\sqrt{\frac{15}{4}}\left\{-\frac{1}{2}\left[\frac{1}{\sqrt{5}}\,(Y_3^{-3} - Y_3^{3}) + \frac{1}{\sqrt{3}}\,(Y_3^{1} + Y_3^{-1})\right]\right\}$$

$$\chi_7 = R(r)\,\sqrt{\frac{15}{4}}\left\{-\frac{i}{2}\left[\frac{1}{\sqrt{5}}\,(Y_3^{-3} + Y_3^{3}) + \frac{1}{\sqrt{3}}\,(Y_3^{1} - Y_3^{-1})\right]\right\}$$

$$\chi_8 = R(r)\,\sqrt{\frac{15}{4}}\left\{\frac{1}{2}\,\sqrt{\frac{8}{15}}\,(Y_3^{2} + Y_3^{-2})\right\}$$

The central ion directed π hybrids are obtained from Eq. (16). Functions ξ_1 and ξ_5 are directed towards ligand "a" which is chosen as the non-bridging oxygen. In the proposed model, only these π hybrids are utilized.

While the introduction of the directed π hybrids permits consideration of π bonding in the non-bridging oxygens only, it is aniticipated that the orthogonality crite.ion might not be sufficiently well satisfied by these hybrids. These π functions are, of course, orthogonal to σ hybrids on their own center. But it is possible that the Si centered π hybrids will have non-negligible overlap with the oxygen σ bonding lobe directed toward the central ion. It will therefore be necessary to evaluate this overlap for comparison with other bond overlaps; a comparison with the overlap of a Si σ hybrid with an oxygen p_x or p_y function (or the equivalent complex functions) for example, should provide insight into the significance of the anticipated non-orthogonality. If this overlap is found to be significant, then a further orthogonalization will be required. This can be accomplished by Löwdin's method of symmetric

orthogonalization.[26] Löwdin has shown that if the functions $\chi\alpha$ institute a non-orthogonal set then the functions Φ_μ defined by the relation

$$\underset{\sim}{\Phi} = \chi \left(\underset{\sim}{1} + \underset{\sim}{S}\right)^{-\frac{1}{2}} \tag{25}$$

are orthogonal and normalized.

The matrix $\underset{\sim}{S}$ is the matrix of overlap integrals. In practice it is usually sufficient to retain only the first terms in the expansion of $(\underset{\sim}{1} + \underset{\sim}{S})^{-\frac{1}{2}}$. One obtains the approximate expression

$$\underset{\sim}{\Phi}_\mu = \underset{\sim}{\chi}_\mu - \frac{1}{2} \sum_\alpha \chi_\alpha S_{\alpha\mu} \tag{26}$$

4.6 COMPUTATIONAL DETAILS - PRESENT STATE OF THE RESEARCH

In the foregoing discussion some formal aspects of the tetrahedral structure calculation have been outlined. There remains a heavy load of computation, most of which centers around the evaluation of the numerous integrals required in Eq. (9). A number of approximations have been made in an attempt to reduce the labor as much as possible without doing excessive violence to the theory. The introduction of directed π orbitals, and the decision to treat second neighbors in a point ion model leads to one- and two-center integrals only. In first approximation, the oxygen nucleus plus $1s^2$ $2s^2$ $2p^6$ shells are to be treated as point charges. Radial functions are to be represented by Slater type orbitals, with all valence functions orthogonalized to the cores.

Except for the orthogonality conditions, there are no restrictions on the orbitals A_i and B_i. To take into account the heteronuclear nature of the complex, bond functions with an ionic component are used. We employ localized molecular orbitals given by the relation

$$A_i = B_i = \Phi_O + \lambda \Phi_{Si} \tag{27}$$

where Φ_O and Φ_{Si} are oxygen and silicon functions and λ is a variational parameter to be determined by minimization of the total energy $\langle \mathcal{H} \rangle$. In this approximation, the spatial part of the two-electron bond function has the form

$$\Phi_O(1)\,\Phi_O(2) + \lambda^2\,\Phi_{Si}(1)\,\Phi_{Si}(2) + \lambda\left[\Phi_O(1)\,\Phi_{Si}(2) + \Phi_O(2)\,\Phi_{Si}(1)\right] \tag{28}$$

Such a function includes electron correlation by allowing an ionic contribution to the bond. In the case where both σ and π bonds are allowed, there are, of course, two variational parameters to be determined.

Explicit evaluation of the molecular integrals is the major problem remaining. During the remainder of the contract period, effort will be devoted to obtaining computer programs and carrying out the structural calculation. Fortran language programs for evaluating one- and two-center integrals which appear in diatomic molecule calculations are distributed through the Quantum Chemistry Program Exchange at Indiana University. As a first step these programs will be obtained and studied to determine their usefulness in the present application and their adaptability to existing computer facilities.

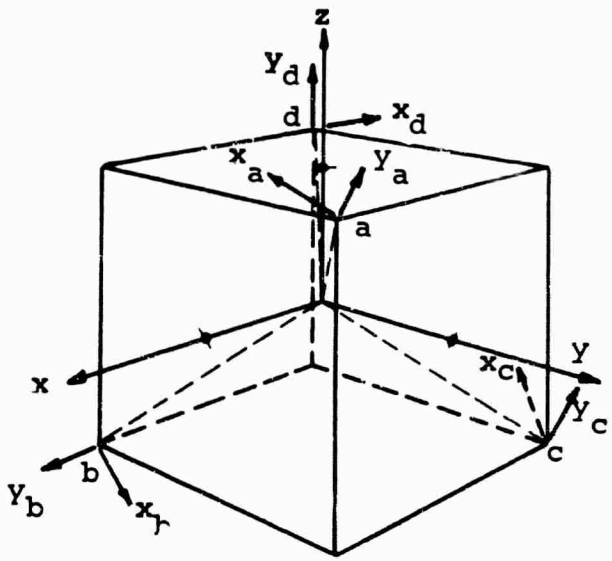

Fig. 20. Coordinates used in evaluating tetrahedral wavefunctions. The orientation of the axes at sites a, b, c, and d relative to the coordinate system originating at the center of the cube is specified in the text.

REFERENCES

1. R. J. Landry, J. T. Fournier and C. G. Young, J. Chem. Phys. 46, 1285 (1967).

2. J. B. Mock. Rev. Sci. Instr., 31, 551 (1960).

3. N. S. Ganif yanov, Soviet Phys. - Solid State, 4, 1795 (1963).

4. L. L. van Reijan, "Electron Spin Resonance Studies of Pentavalent and Trivalent Chromium," (Doctoral Thesis, Technological University at Eindhaven, 1964).

5. J. S. Griffith, The Theory of Transition Metal Ions, (Cambridge University Press, London, 1961).

6. M. M. Abraham, J. P. Alviata, M. E. Foglio, and E. Pasquini, J. Chem. Phys. 45, 2069 (1966).

7. L. Pauling, The Nature of the Chemical Bond, (Cornell University Press, Ithaca, New York, 1945), pp. 346, 350.

8. A. Abragam and M. H. L. Pryce, Proc. Roy. Soc. (London) A205, 135 (1951).

9. I. Siegel and J. A. Lorenc, J. Chem. Phys., 45, 2315 (1966).

10. T. Bates, Ligand Field Theory and Absorption Spectra of the Transition Metal Ions, in J. D. Mackenzie, ed., Modern Aspects of the Vitreous State. (Butterworths, London, 1962), Vol. 2, P. 195.

11. W. Shiner, E. Snitzer, and R. F. Woodcock, Phys. Letters 4, 412 (1966).

12. A. Kats and J. M. Stevels, Philips Research Reports, 11, 115 (1956).

13. Rinda Allison and Jay Burns, J. Opt. Soc. of America, 55, 574 (1965).

14. J. W. Schreurs and R. F. Tucker. Proc. Intern. Conf. on Physics of Noncrystalline Solids, J. A. Prins Ed. (North-Holland Publishing Co., Amsterdam), 1965, P. 616.

15. D. M. Yudin, Soviet Phys. - Solid State 1, 1733 (1965).

16. P. Beekenkamp, Philips Research Reports Supplements, No. 4, 1966.

17. J. W. Schreurs, Bull. Am. Phys. Soc., Jan. 1967, P. 42.

18. B. E. Warren, H, Krutter and O. Morningstar J. Am. Ceram. Soc. 19, 202 (1936).

19. A. C. Hurley, J. E. Lennard-Jones, and J. A. Pople, Proc. Roy. Soc. (London) A220, 446 (1953.

20. J. C. Slater Quantum Theory of Molecules and Solids, Vol. 1 (McGraw-Hill Book Co., Inc., New York, 1963), P. 198, Appendix 14.

21. C. A. Coulson, L. B. Rèdei, and D. Stocker, Proc. Roy. Soc. (London) A270, 357 (1963).

22. J. H. Van Vleck, J. Chem. phys. 3, 803 (1935).

23. G. F. Koster, Phys. Rev. 109, 227 (1958).

24. J. C. Slater, QTMS, Vol. 1, P. 358.

25. J. C. Slater, QTMS, Vol. 1, P. 160.

26. P. O. Löwdin, J. Chem. Phys. 18, 365 (1950).

27. Measurements of R. Mozzi reported by B. E. Warren at the New York Conference of the American Ceramic Society, 1967.

Unclassified

Security Classification

DOCUMENT CONTROL DATA - R&D

(Security classification of title, body of abstract and indexing annotation must be entered when the overall report is classified)

1. ORIGINATING ACTIVITY (Corporate author)	2a. REPORT SECURITY CLASSIFICATION
Research Division American Optical Company Southbridge, Massachusetts 01550	Unclassified
	2b. GROUP N/A

3. REPORT TITLE

ESR and Optical Absorption Studies of Transition Metal Ions and Color Centers in Glass

4. DESCRIPTIVE NOTES (Type of report and inclusive dates)

Semi-Annual Technical Report No.1, 1 October - 31 March 1967

5. AUTHOR(S) (Last name, first name, initial)

Landry, Robert J.

Fournier, Joseph T.

6. REPORT DATE	7a. TOTAL NO. OF PAGES	7b. NO. OF REFS
June 1967	51	26

8a. CONTRACT OR GRANT NO.	9a. ORIGINATOR'S REPORT NUMBER(S)
N00014-67-C-0186	TR 599-1
b. PROJECT NO. ARPA ORDER 306	
c.	9b. OTHER REPORT NO(S) (Any other numbers that may be assigned this report) N/A
d.	

10. AVAILABILITY/LIMITATION NOTICES

Qualified requestors may obtain copies of this report from DDC. Distribution of this document is unlimited.

11. SUPPLEMENTARY NOTES	12. SPONSORING MILITARY ACTIVITY
Research is part of Project DEFENDER	Office of Naval Research Department of the Navy Washington, D. C.

13. ABSTRACT

The theory of zero field ESR measurements of an S = 3/2 system is considered, including spectrometer considerations. A brief discussion of an experimental problem associated with temperature dependent ESR intensity measurements of broad powder spectra is included along with a proposed solution. The optical absorption and ESR spectra of Mo^{3+} and Cu^{2+} in glass, in the concentration range 0.1-16.0 wt. % MoO, and CuO, respectively, were investigated. In both cases, the ESR spectra are found to be concentration dependent. For isolated Cu^{2+}, the axial spin Hamiltonian parameters obtained are: $g_{\parallel} = 2.335 \pm 0.002$, $g_{\perp} = 2.050 \pm 0.001$, $A_{\parallel} = 155 \pm 1 \times 10^{-4} cm^{-1}$, and $A_{\perp} = 22.7 \pm 0.1 \times 10^{-4} cm^{-1}$. ESR and optical absorption spectra of Mo^{3+} in a phosphate glass are shown. The value of the crystal field splitting parameter Δ is $22,000/cm^{-1}$, about 52% greater than the value of $14,500/cm^{-1}$ for isoelectronic Cr^{3+} in the same base glass.[1] The spin resonance spectra of Cr^{3+} and Mo^{3+} are compared, from which it is concluded that they are similarly accommodated in the glass. Their local environments appear to be identical. A technique is described which allows for a precise determination of the activation spectrum for production of permanent color center defects by ultraviolet light. The activation spectrum for induced permanent color center defects in a laser base glass is presented. The spectrum has a peak at 214 nm and has a full width at half maximum of 150 nm. An upper bound of 240 nm for the activation spectrum for short lived laser Q-switching color center defects is demonstrated.

Preliminary results of a theoretical investigation of the electronic structure of color center defects associated with network-forming tetrahedra are reported. A silicon-oxygen tetrahedron with a single non-bridging oxygen is chosen as the initial subject for study. The molecular structure of the tetrahedron is described in the valence bond picture, and a formal discussion of valence bond theory is presented. The role of π bonding in the tetrahedron is considered. It is shown that localized π hybrids can be constructed from Si 3d and 4f atomic orbitals, and the details of a group theoretical procedure for determining these hybrids are presented. Finally, some computational aspects of the problem are discussed.

DD FORM 1 JAN 64 1473

Unclassified

Security Classification

14. KEY WORDS	LINK A		LINK B		LINK C	
	ROLE	WT	ROLE	WT	ROLE	WT
Glass Glass Structure Laser Glass Lasers ESR Measurements Color centers						

INSTRUCTIONS

1. ORIGINATING ACTIVITY: Enter the name and address of the contractor, subcontractor, grantee, Department of Defense activity or other organization *(corporate author)* issuing the report.

2a. REPORT SECURITY CLASSIFICATION: Enter the overall security classification of the report. Indicate whether "Restricted Data" is included. Marking is to be in accordance with appropriate security regulations.

2b. GROUP: Automatic downgrading is specified in DoD Directive 5200.10 and Armed Forces Industrial Manual. Enter the group number. Also, when applicable, show that optional markings have been used for Group 3 and Group 4 as authorized.

3. REPORT TITLE: Enter the complete report title in all capital letters. Titles in all cases should be unclassified. If a meaningful title cannot be selected without classification, show title classification in all capitals in parenthesis immediately following the title.

4. DESCRIPTIVE NOTES: If appropriate, enter the type of report, e.g., interim, progress, summary, annual, or final. Give the inclusive dates when a specific reporting period is covered.

5. AUTHOR(S): Enter the name(s) of author(s) as shown on or in the report. Enter last name, first name, middle initial. If military, show rank and branch of service. The name of the principal author is an absolute minimum requirement.

6. REPORT DATE: Enter the date of the report as day, month, year; or month, year. If more than one date appears on the report, use date of publication.

7a. TOTAL NUMBER OF PAGES: The total page count should follow normal pagination procedures, i.e., enter the number of pages containing information.

7b. NUMBER OF REFERENCES: Enter the total number of references cited in the report.

8a. CONTRACT OR GRANT NUMBER: If appropriate, enter the applicable number of the contract or grant under which the report was written.

8b, 8c, & 8d. PROJECT NUMBER: Enter the appropriate military department identification, such as project number, subproject number, system numbers, task number, etc.

9a. ORIGINATOR'S REPORT NUMBER(S): Enter the official report number by which the document will be identified and controlled by the originating activity. This number must be unique to this report.

9b. OTHER REPORT NUMBER(S): If the report has been assigned any other report numbers *(either by the originator or by the sponsor)*, also enter this number(s).

10. AVAILABILITY/LIMITATION NOTICES: Enter any limitations on further dissemination of the report, other than those imposed by security classification, using standard statements such as:

(1) "Qualified requesters may obtain copies of this report from DDC."

(2) "Foreign announcement and dissemination of this report by DDC is not authorized."

(3) "U. S. Government agencies may obtain copies of this report directly from DDC. Other qualified DDC users shall request through _____."

(4) "U. S. military agencies may obtain copies of this report directly from DDC. Other qualified users shall request through _____."

(5) "All distribution of this report is controlled. Qualified DDC users shall request through _____."

If the report has been furnished to the Office of Technical Services, Department of Commerce, for sale to the public, indicate this fact and enter the price, if known.

11. SUPPLEMENTARY NOTES: Use for additional explanatory notes.

12. SPONSORING MILITARY ACTIVITY: Enter the name of the departmental project office or laboratory sponsoring *(paying for)* the research and development. Include address.

13. ABSTRACT: Enter an abstract giving a brief and factual summary of the document indicative of the report, even though it may also appear elsewhere in the body of the technical report. If additional space is required, a continuation sheet shall be attached.

It is highly desirable that the abstract of classified reports be unclassified. Each paragraph of the abstract shall end with an indication of the military security classification of the information in the paragraph, represented as *(TS), (S), (C), or (U)*.

There is no limitation on the length of the abstract. However, the suggested length is from 150 to 225 words.

14. KEY WORDS: Key words are technically meaningful terms or short phrases that characterize a report and may be used as index entries for cataloging the report. Key words must be selected so that no security classification is required. Identifiers, such as equipment model designation, trade name, military project code name, geographic location, may be used as key words but will be followed by an indication of technical context. The assignment of links, roles, and weights is optional.